$^{40}Ar/^{39}Ar$ Diffusion and Age Constraints in Muscovite from the Ruby Mountains, Northeastern Nevada

by

Kayla M. Griffin

A thesis submitted to the Graduate Faculty of
Auburn University
in partial fulfillment of the
requirements for the Degree of
Master of Science

Auburn, Alabama
August 4, 2018

Approved by

Willis E. Hames, Chair, Professor of Geosciences
Mark G. Steltenpohl, Professor of Geosciences
Dmitry V. Glotov, Associate Professor of Mathematics and Statistics

Abstract

Plutonic rocks exposed in the Basin and Range province are known to have experienced widespread extension and uplift at ca. 16.5 Ma. This extension is broadly coincident with timing of earliest volcanism of the Yellowstone hotspot (notably in the Northern Nevada rift and Oregon-Idaho graben and manifest by widespread basalts of the early Columbia River basalt province). Although the coincidence in timing leads to suggestions of a causal relationship, the overall magnitude and history of pre-early Miocene cooling and exhumation of mid- to deep-level crust is unclear. One reason for this existing uncertainty is that most of the geochronologic data available in central and eastern Nevada are for volcanic rocks and low temperature (<200°C) thermochronometers. The Ruby Mountains East Humboldt (RMEH) metamorphic core complex exposes deep crustal sections in the eastern Basin and Range province that have been the subject of extensive previous study. Previous published studies focused on low-temperature history (e.g. Colgan et al. [*2010*]) and emphasize a mid- to late-Miocene episode of exhumation that might coincide with the early Yellowstone hotspot [*Camp et al., 2015*]. The published thermochronologic data for the RMEH bearing on the higher temperature exhumation history, prior to the mid-Miocene, are insufficient to provide an unambiguous evaluation of the early exhumation history of the Ruby Mountains. It is critical to understand the pre-early Miocene exhumation history of this region in order to properly evaluate competing hypotheses for the origin of regional extension in the Ruby Mountains, such as I) decompression of over-thickened crust following the Sevier orogeny, or II) uplift caused by the Miocene Yellowstone hotspot.

Samples were collected from traverse and longitudinal sections of the Ruby Mountains metamorphic core complex for single-crystal $^{40}Ar/^{39}Ar$ dating, with emphasis on muscovite, in order to provide new constraints to the ca. 450-300°C thermal history of deep crustal sections presently exposed in the RMEH. Samples were prepared for analysis in the ANIMAL facility, and include relatively undeformed, euhedral muscovite phenocrysts up to 2 mm in diameter that were collected from syn- to post-kinematic granitic intrusives. Using single crystal fusion, muscovite and biotite crystals from the Ruby Mountains were determined to have $^{40}Ar/^{39}Ar$ ages of approximately 35-30 Ma in locations in the eastern Ruby Mountains, 26-25 Ma in central locations, and 22-20 Ma in northern and western locations in the footwall near the detachment fault. The data suggests unroofing of the RMEH metamorphic and igneous basement lithologies and retention of $^{40}Ar^*$ in micas began by ca. 35 Ma to the east, and progressed to final closure of $^{40}Ar^*$ in micas by ca. 20 Ma in the west. In contrast to the regional variation of up to ca. 17 million years in cooling ages, cooling through the $^{40}Ar^*$ closure interval seemed to have occurred at rapid rates (ca. 30°C/m.y. or higher) in any particular sample location. The new data are best reconciled with ages published previously for crystallization of zircon and monzanite in felsic intrusives and low-temperature thermochronometers by cooling during ongoing extension with rapid uplift in the Oligocene and early Miocene. The present study derives cooling rates from the $^{40}Ar/^{39}Ar$ ages of single mica crystals, with closure temperatures calculated on the basis of the crystal size. The ages and calculated closure temperatures were used to further constrain cooling histories of the Ruby Mountains and formulate a more complete time-temperature model. Most of the extension that formed the metamorphic complex occurred before regional extension that could have arisen from the upwelling of the Yellowstone hotspot, and thus was not driven by Yellowstone volcanism.

Acknowledgments

This project received funding by the Geosciences Advisory Board, the Spencer Waters and Dan Folse Memorial Award, and the Auburn Noble Isotope Mass Analysis Labratory. I would like to give thanks to Dr. Bill Hames, who has given me patience, support, and guidance throughout my research. I would also like to thank the rest of my committee members, Dr. Mark Steltenpohl, Dr. Haibo Zou, and Dr. Dmitry Glotov, for their thoughts and suggestions on my thesis. Thank you to Ben Smith and Justin Ryerse for their help during field work in summer 2016. Thank you to Dr. Art Snoke for providing two samples (T5 and 554-34). I would also like to give special thanks to my God, my wonderful family, and my dear friends, who have given me continuous love and support throughout the writing process as well as my academic career.

Table of Contents

List of Tables

List of Figures

List of Abbreviations

RMEH	Ruby Mountains East Humboldt
HP	Harrison Pass
SP	Secret Pass
LC	Lamoille Canyon
CMT	Colonel Moore Trailhead
EMPA	Electron Microprobe Analysis
ANIMAL	Auburn University Noble Isotope Mass Analysis Laboratory

1 INTRODUCTION

1.1 Exhumation and Extension

Exhumation, or the exposure of crustal rocks, can be associated with several different processes including continental convergence and the upwelling of a mantle plume. It is driven primarily by extension, a tectonic process associated with the stretching of the lithosphere. It occurs in areas such as rifts in divergent plate boundaries where the crust is being pulled apart, but it can also occur at convergent plate boundaries. Figure 1 shows different tectonic mechanisms experienced by the crust. At convergent plate boundaries, as shown in Figure 1A, the crust thickens vertically forming a crustal root and a high plateau. This eventually becomes weaker due to gravitational instability and spreads out, forming normal faults and exposing the deep rocks from the crustal root [*England*, 1982]. Figure 1B depicts a divergent plate boundary. This is another area driven by extension at which the crust is stretching. The stretching of the crust results in many normal faults. Extension can also occur in the crust above mantle plumes as shown in Figure 1C. The plume can begin to form a dome, upwelling and resulting in the stretching and splitting of the crust above it.

1.2 Metamorphic Core Complexes

Metamorphic core complexes are areas where deep crustal rocks have been exposed. Formation of metamorphic core complexes within the Basin and Range has been debated by geologists, and it has been associated with widespread magmatism [*Armstrong and Ward, 1991*] and crustal thickening followed by extension [*Coney and Harms, 1984*]. Figure 2 shows

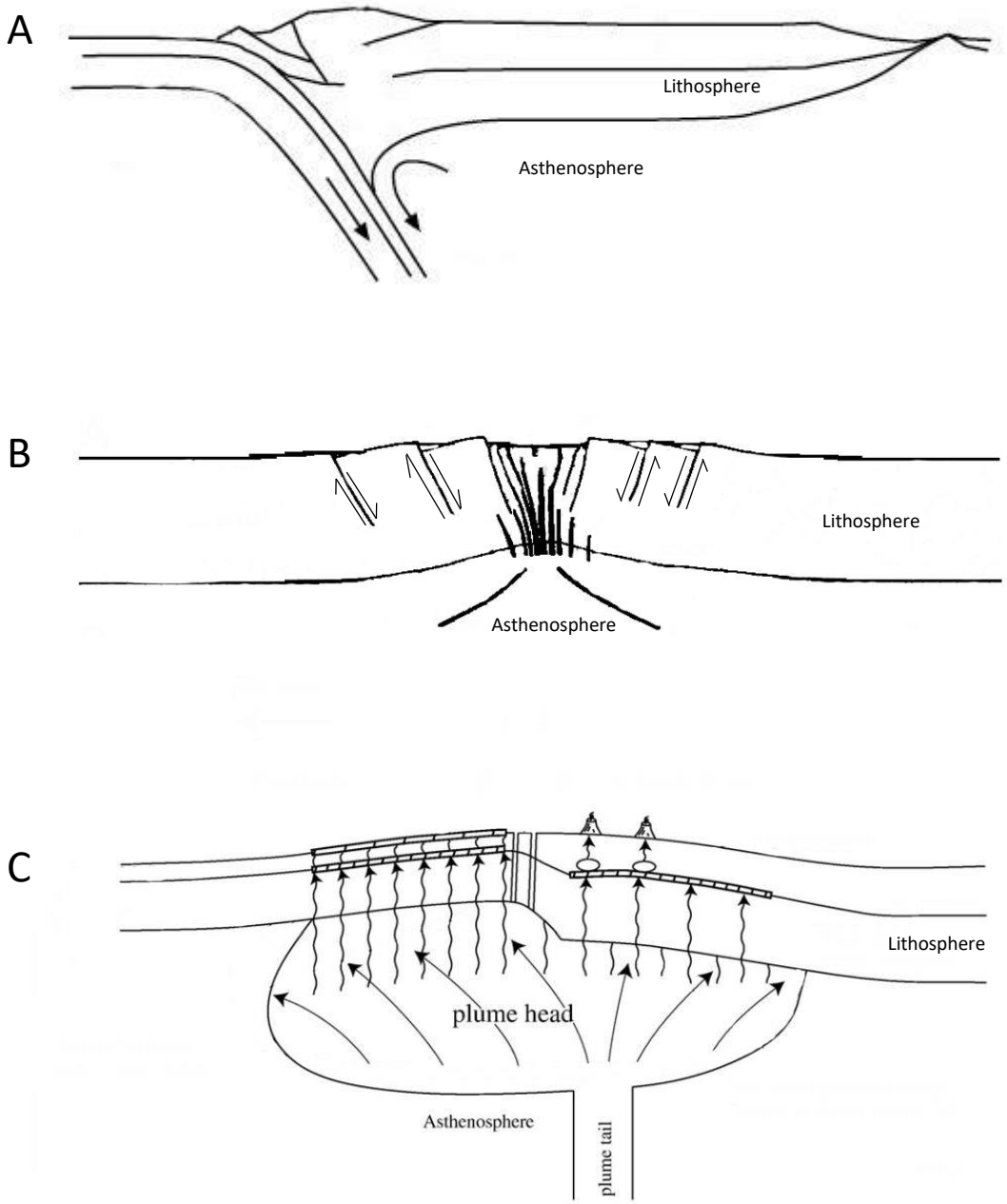

Figure 1. Three diagrams of tectonic mechanisms experienced by the crust. A: Convergent plate boundary at which the crust is thickening, forming a high plateau [modified from *Decelles*, 2004]; B: Divergent plate boundary at which the crust is stretching, resulting in many normal faults [modified from *Dewey and Bird.*, 1970]. C: Mantle plume head upwelling beneath the crust, resulting in crustal thinning, intrusions into the crust, and lava flows [modified from *Pierce and Morgan*, 1992].

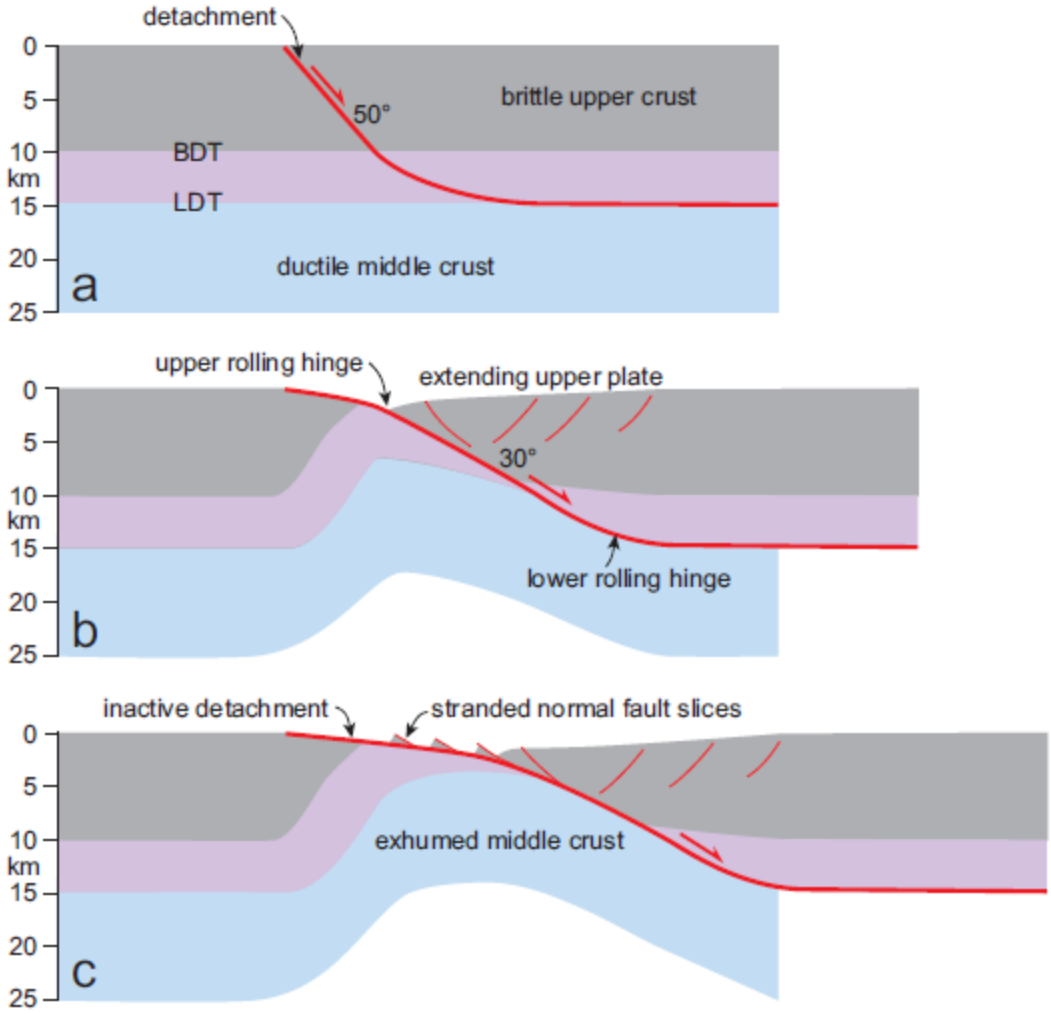

Figure 2. a. detachment forms at high angle and runs through the brittle-ductile transition (BDT) to the transition from localized to distributed ductile deformation (LDT). b. as the plate stretches, dip of the detachment is reduced. c. rollover of the detachment. Figure from *Platt et al.*, 2015.

.

the evolution of a metamorphic core complex along a detachment fault. The Ruby Mountain East Humboldt Range (RMEH) is a metamorphic core complex in northeastern Nevada that is useful for studying geologic history for the area in the Basin and Range (Figure 3). The RMEH has been chosen for this work because of the exposure of igneous and metamorphic rocks throughout the range. Mineral phases from these rocks can be dated, and a local and regional geologic history can be interpreted. Determining the geologic history of the RMEH can help determine whether extension in the mountain range as well as regional extension occurred due to the upwelling of the Yellowstone mantle plume, or if it can be attributed to some other mechanism.

1.3 The Basin and Range Province

Thrust faulting that occurred in western North America during the Middle Jurassic to early Tertiary resulted in an overthickened crustal welt in the hinterland [*Coney and Harms,* 1984*; DeCelles*, 2004]. This was termed the "Nevadaplano" by DeCelles [2004] and is shown in Figure 3. The Basin and Range Province is a region encompassing eight states in western North America. It is characterized by its topography displaying parallel mountain ranges and alternating basins formed by extension of thickened crust and bimodal volcanism. The extension became widespread at approximately 17 Ma [*John*, 2001], though it started earlier and was probably driven by heating [*Eaton,* 1982]. The driving mechanisms of extension in the Basin and Range Province have been debated, and popular explanations include gravitational collapse of an overthickened crust [*Dewey,* 1988] and the upwelling of the Yellowstone Hotspot [*Pierce and Morgan,* 1992*; Parsons et al.,* 1994*; Saltus and Thompson,* 1995*; Camp et al.,* 2015].

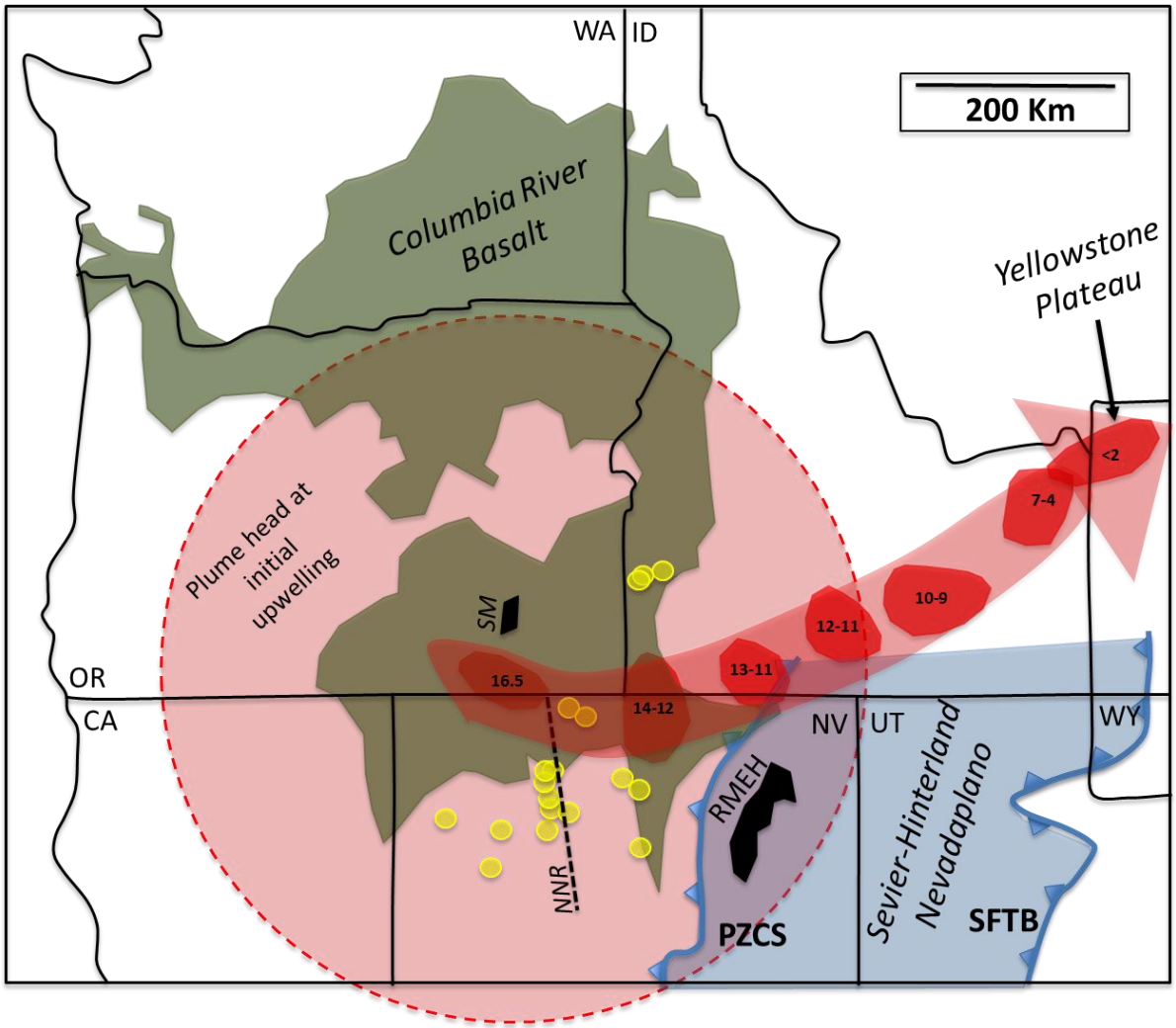

Figure 3. Generalized map showing the location of the Northern Nevada Rift, basalt flows of the Columbia River Large Igneous Province, Ruby Mountains, and Nevadaplano [*Decelles,* 2004] in the context of the Miocene Yellowstone hotspot plume head. Progressive centers of the Yellowstone hotspot are outlined in red [*Pierce and Morgan,* 1992; *Brueseke et al.,* 2007]. Locations of current and historic gold mines are shown as yellow circles. Abbreviations: SM – Steens Mountain; NNR – Northern Nevada Rift; RMEH – Ruby Mountains East Humboldt Metamorphic Core Complex; SFTB – Sevier Fold and Thrust Belt; PZCS – Paleozoic Carbonate Shelf. Figure modified from *Pierce and Morgan,* 1992; *Brueseke et al.,* 2007; *Hames et al.,* 2009; *Snell et al.,* 2014, and the University of Utah[1].

[1]Yellowstone Hotspot Overview website created by the University of Utah. http://www.yellowstonegis.utah.edu/research/hotspot.html

1.4 Initiation of the Yellowstone Hotspot

The center of the initial upwelling of the Yellowstone hotspot is located in the Basin and Range. The upwelling also occurred at approximately 17 Ma. Because of this, it has been suggested that the extension was caused by the upwelling of the plume [*Pierce and Morgan,* 1992; *Camp et al.,* 2015]. The estimated diameter of the plume at initial upwelling as well as the migration of the center of the plume is depicted on Figure 3. The estimated diameter of the plume head at initial upwelling encompasses the location of the Ruby Mountains East Humboldt Range, which is in northeastern Nevada.

1.5 Statement of Hypothesis

Through single crystal fusion $^{40}Ar/^{39}Ar$ dating of muscovite from the Ruby Mountains, this study will further constrain the geologic history of the area. Muscovite has a higher closure temperature than the mineral phases used for many previous studies, and the data produced will be used to determine cooling rates at temperatures above 350°C. Cooling rates will be calculated on the basis of observed ranges in mineral grain diameters. Although measurements of grain diameters have been considered in studies with other thermochronologic techniques (especially for the (U-Th)/He dating, of apatite), variations in grain diameters for single rock samples are not typically used to estimate closure temperatures for $^{40}Ar/^{39}Ar$ dating. The assessment of potential grain diameter effects for $^{40}Ar/^{39}Ar$ dating will provide a novel way to approach interpretations of Ar data. A temperature-time path will be produced from which depth will be inferred. This information will help determine whether extension in the Ruby Mountains, Nevada was driven by the upwelling of the Yellowstone Hotspot or another tectonic mechanism.

2 GEOLOGIC SETTING

2.1 Previous Age Dating Work on the Ruby Mountains

The Ruby Mountain-East Humboldt Range (RMEH) is a metamorphic core complex located in northeastern Nevada, US. It is on the Nevadaplano in the Sevier-Hinterland (Figure 3), and lies west of the Sevier fold and thrust belt. Samples from the northernmost region of the East Humboldt range suggest metamorphism during the Cretaceous at depths of approximately 37-39 km [*Hodges et al.,* 1992]. The exposed igneous and metamorphic rocks within the RMEH record episodes of extension and exhumation along a ~20° west dipping brittle detachment fault [*Colgan et al.,* 2010]. This fault as well as other low angle normal faults overlie a west-northwest trending shear zone that is superimposed on amphibolite facies migmatitic rocks [*Dallmeyer et al.,* 1986; *Dokka et al.,* 1986]. Extension along the detachment fault occurred into the Miocene, and there was a rapid uplift event that occurred at approximately 16.5 Ma [*Snoke and Miller,* 1988; *Colgan et al.,* 2010]. A generalized geologic map depicting the location of the detachment fault as well as the mylonitic shear zone and igneous rocks in the RMEH is shown in Figure 4.

Dallmeyer et al. [1986] presented results for approximately thirty K/Ar and $^{40}Ar/^{39}Ar$ analyses in a study of the Ruby Mountains-East Humboldt Range. They reported hornblende and biotite ages from different locations within the Ruby Mountains. The hornblende ages varied widely — with ages reported as old as 218 ± 8 Ma to as young as 31.4 ± 1.4 Ma. The biotite ages range from 33.7 ± 1.1 Ma to 20.8 ± 0.5 Ma. Apatite, zircon, and sphene fission track ages were

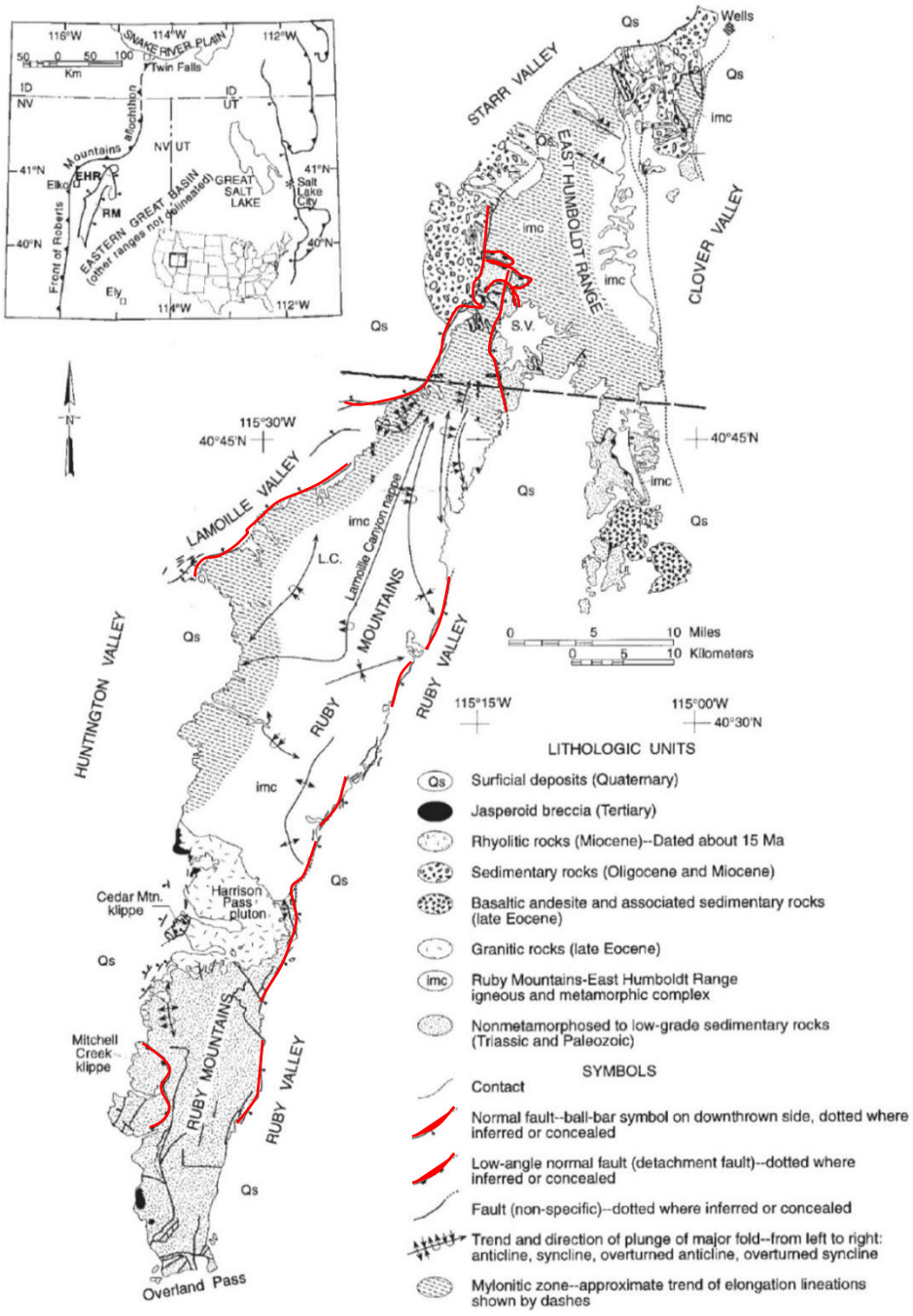

Figure 4. Generalized geologic map of the Ruby Mountains, Nevada. Map is adapted from MacCready et al. [1997].

reported by Dokka et al. [1986]. These ages ranged from Oligocene to early-Miocene, and they interpreted a rapid cooling event that unroofed mid-crustal rocks at approximately 25-23 Ma. U-Pb zircon and monzonite crystals from intrusive granitic rocks were reported to have ages of approximately 40-29 Ma by Wright and Snoke [1993]. From these data, they interpreted significant and widespread magmatism during this time [*Wright and Snoke,* 1993]. Zircon and Monzanite U-Pb ages from mid-crustal leucogranites were reported by Howard et al. [2011]. Ages were found to range from 92-29 Ma, and this was interpreted as multiple episodes of melting and crystallization [*Howard et al.,* 2011].

The Harrison Pass pluton (Figure 4) exposes Miocene plutonic rocks that were initially uplifted and cooled during the Oligocene [*Kistler et al.,* 1981*; Colgan et al.,* 2010]. Colgan and others [2010] also concluded that they were unroofed by slip of a detachment fault from about 17 Ma to 10-12 Ma. Illite ages of 11-13 Ma for fault gouge reported by Haines and Van Der Pluijm [2010] provides evidence that supports the suggestion that exhumation and faulting continued into and ended in the late Miocene.

The thermochronologic data from previous studies are summarized in Figure 5. Given the existing data, different Temperature-time paths can be produced, and three are drawn (Figure 5). Path 1 would imply more rapid cooling in the Cretaceous, and then slow cooling at a mid-crustal level until around 35 Ma. After 35 Ma, the path would require more rapid cooling and exhumation. This history would require early Cretaceous exhumation followed by 40 m.y. of residence at a depth of approximately 10-15 km (assuming a gradient of 30°/km). However, this path does not encompass the timing of many of the reported ages. Path 3 would require lithologies to have resided at approximately 20 km depths until rapid cooling in the Eocene into

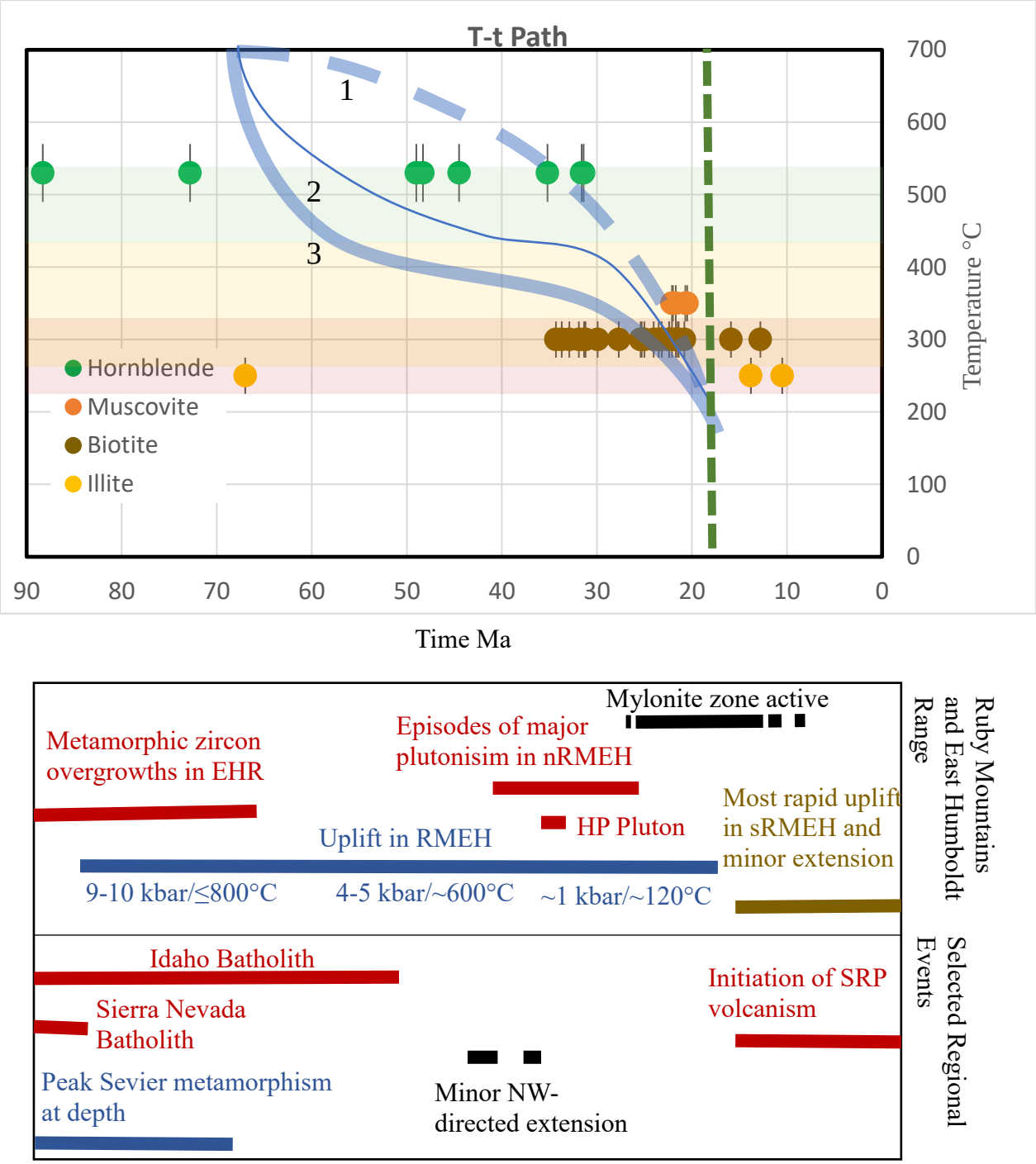

Figure 5. A: Temperature-time graph compiled using data from Dallmeyer et al. [1986], McGrew and Snee [1994], Haines and Van Der Pluijm [2010], and Colgan et al. [2010]. Three possible paths are shown, as discussed in the text. The green dashed line represents timing of upwelling of the Yellowstone Hotspot. B: Summary of geologic events modified from Lund Snee et al. [2016]. Abbreviations: EHR – East Humboldt Range, RMEH – Ruby Mountains East Humboldt Range, SRP – Snake River Plain.

the Miocene. Path 2 shows an intermediate history between paths 1 and 3. Each of these paths is plausible, and the present study has been set up to determine and utilize muscovite ages so the correct path can be identified. The sampling and minerals studied in the present work will further constrain these ages and cooling histories and allow a greater understanding of the pre-17 Ma tectonic events that controlled exhumation of the RMEH. This will determine the degree to which extension of the Ruby Mountains is temporally consistent with initiation of volcanism of the Yellowstone hotspot.

2.2 Significance of This Project

New age data for the Ruby Mountains will be reported, along with interpretations of cooling histories for various rocks in that setting. Through the use of muscovite in this study, higher temperature constraints on cooling will be determined, and a T-t path will be further constrained. Through determining ages and cooling histories of minerals from the Ruby Mountains, this study will lead to a greater understanding of the Ruby Mountain detachment as well as the Basin and Range Province, giving insight on any correlation to the timing of events associated with the arrival of the Yellowstone mantle plume. This study will also utilize a novel application for $^{40}Ar/^{39}Ar$ dating through accounting for the relationship of grain diameter on cooling rates. This technique has been used previously in studies with (U-Th)/He dating, as it has been shown that closure temperature and cooling rate is a function of grain diameter in apatite [*Reiners and Farley*, 2001].

3 FIELD SAMPLING

Field work in the Ruby Mountains, Nevada was conducted in July 2016. Twenty-four samples of pegmatite, granite, and amphibolite were collected from a traverse across the central Ruby Mountains as well as from other various latitudes in the RMEH over the course of 3 days. Sample locations include Lamoille Canyon, Liberty Lake, Colonel Moore Trailhead, Secret Pass, and Harrison Pass. These locations are shown on Figure 6. A table of sample information and locations can be found in Appendix A. Photographs of hand samples and outcrop views are provided in Figure 7. Representative photomicrographs of hand samples are provided in Figure 8.

Samples collected from Lamoille Canyon were predominately pegmatites (Figures 7A-7D). Two samples of gneiss were collected as well as one amphibolite from a lens in the gneiss. Sample 16A was taken from a fracture surface near the detachment fault in Lamoille canyon (Figure 7A). It contains large euhedral muscovite crystals and terminated quartz crystals that collectively grew as cavity-filling crystals (Figure 7C). Under a petrographic microscope, these sections showed deformed quartz and muscovite as well as feldspars (Figures 8A and 8B). Pegmatite samples were also collected along the trail to Liberty Lake at the eastern end of Lamoille Canyon. Undeformed granitic samples as well as books of muscovite were collected at Colonel Moore Trailhead on the Eastern side of the Ruby Mountains (Figures 7E-7F).

Samples of deformed granite and gneiss were collected from Secret Pass in the Northern Ruby Mountains and show recrystallized quartz with subrains and undulose extinction and

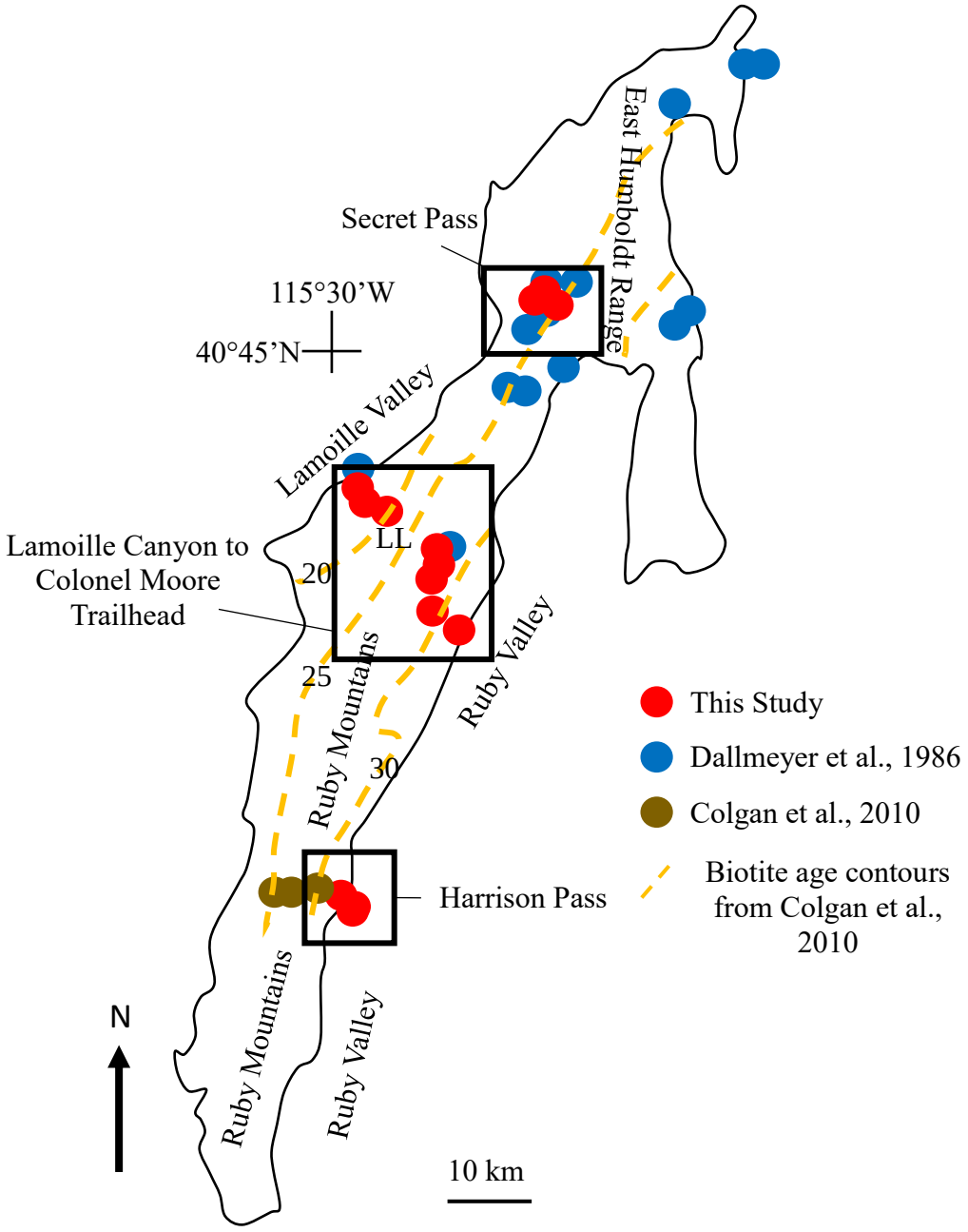

Figure 6. General map of the Ruby Mountains, Nevada. Sample locations of this study are shown as well as those from Dallmeyer et al. [1986] and Colgan et al. [2010]. Yellow dashed lines represent biotite age contours from Colgan et al. 2010. Locations of Secret Pass, Lamoille Canyon to Colonel Moore Trailhead transect, and Harrison Pass are outlined in boxes (See Figures 13, 14, and 15, respectively). Liberty Lake is represented by the 'LL.' Map is redrafted and simplified from MacCready et al. [1997].

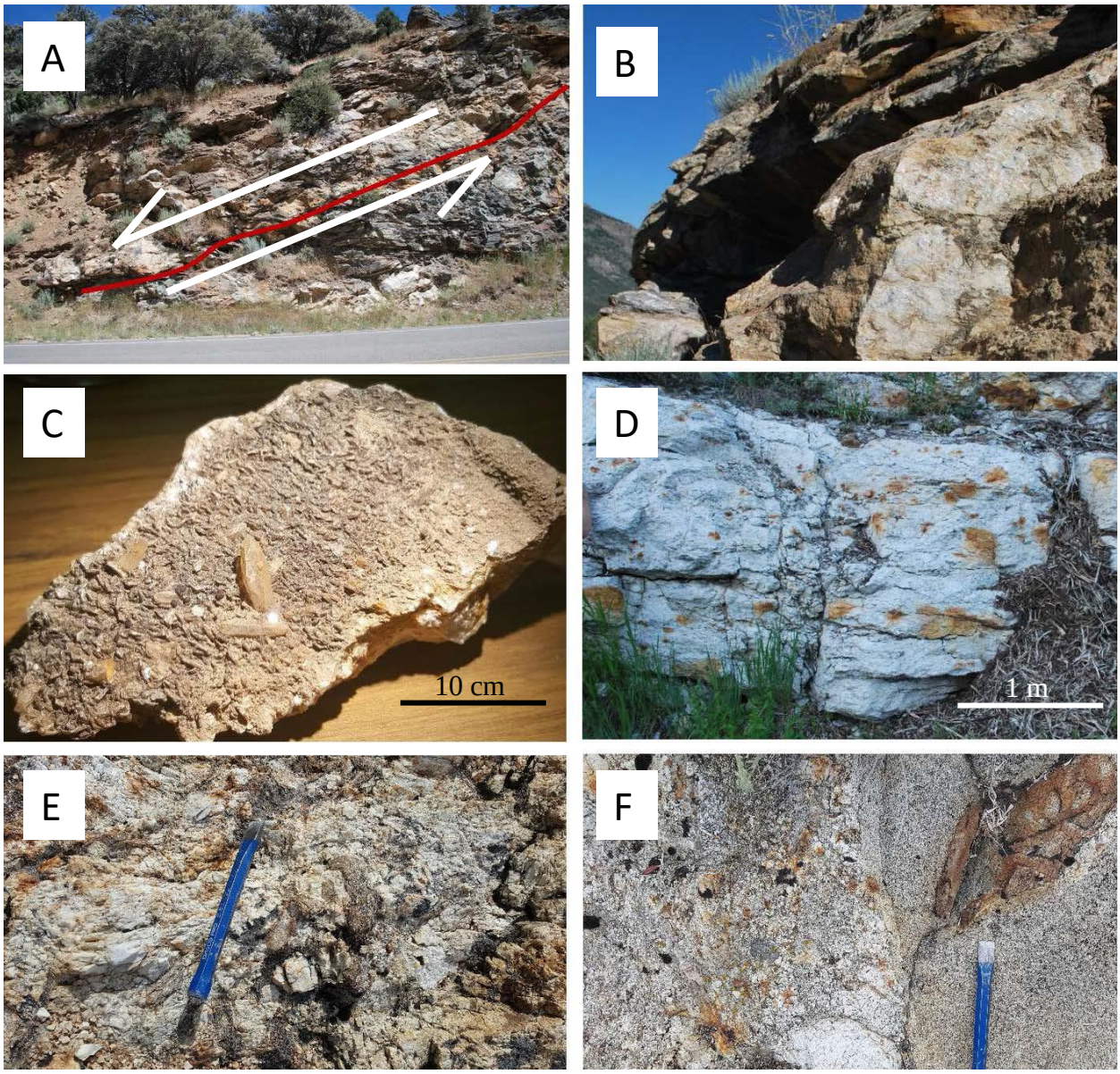

Figure 7. Sampling includes a northwest-southeast transect across the Ruby Mountains along Lamoille Canyon, as represented in these field photos. A: Pegmatite and biotite gneiss layers in contact with amphibolite (footwall) along a detachment fault (red line) in Lamoille Canyon. B: Fracture face on an outcrop in Lamoille Canyon. C: Sample collected from fracture face B. Sample contains euhedral quartz and muscovite, which grew into a fracture cavity and is an ideal sample for dating the timing of fracture formation. D: Pegmatite outcrop in Lamoille Canyon containing coarse crystals of muscovite and microcline. E: Coarse undeformed pegmatite outcrop at Colonel Moore Trailhead. F: undeformed pegmatite in contact with biotite gneiss with pegmatite and gneiss xenolith. Samples show less deformation toward the southeast side of the transect. Chisel=5".

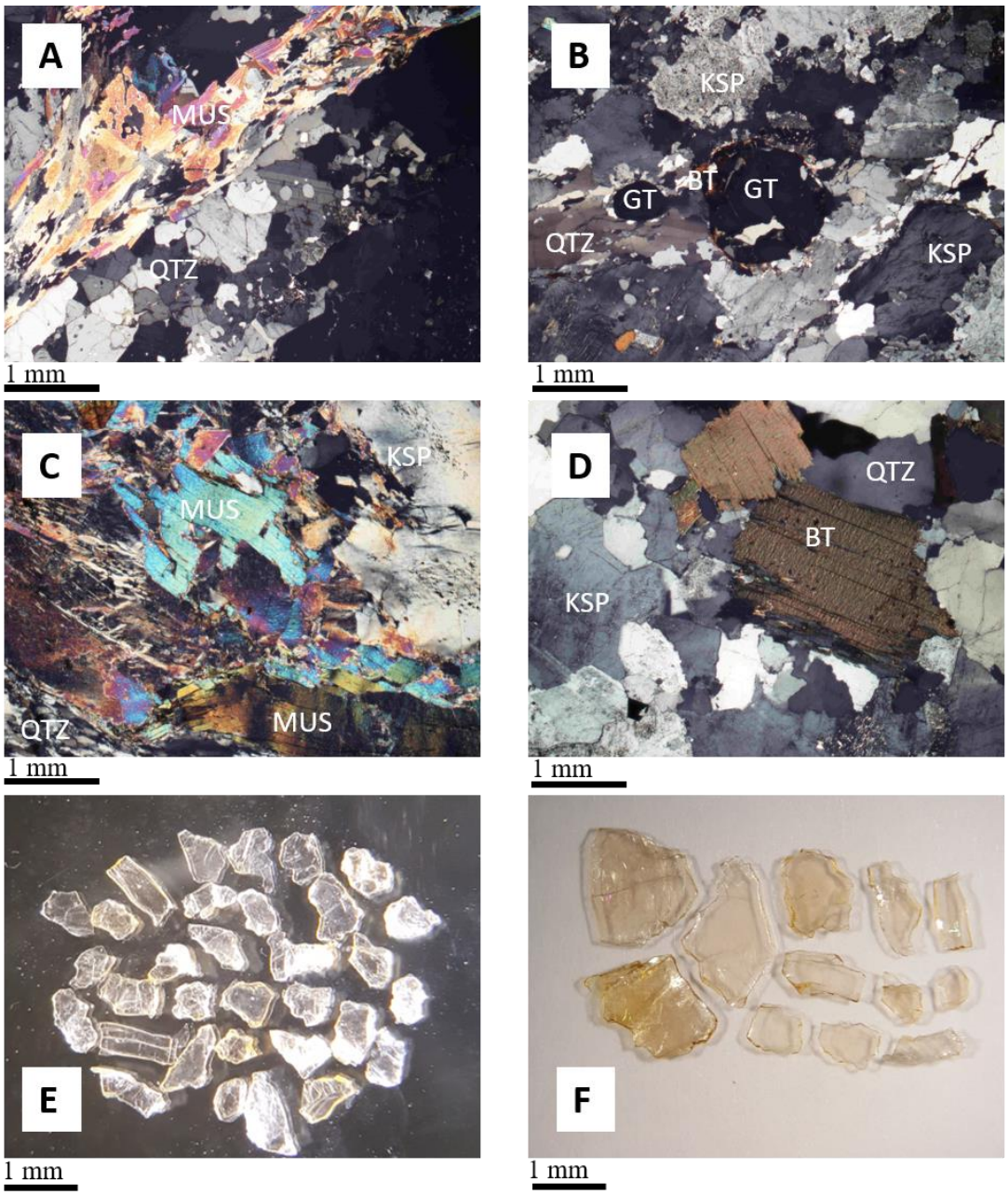

Figure 8. Cross-Polarized Photomicrographs of samples 15, 17A, 8B, 6 from Ruby Mountains. A: Sample 15 from Lamoille Canyon contains deformed quartz and muscovite. B: Sample 17A from Lamoille Canyon contains deformed quartz, potassium feldspar, and garnet with biotite alteration. C: Sample 8B from Secret pass contains recrystallized quartz with subgrains and undulose extinction and kinked muscovite suggesting ductile deformation. D: Sample 6 from Harrison Pass contains undeformed quartz, potassium feldspar, and biotite. E: Undeformed muscovite crystals from sample 20D in Colonel Moore Trailhead ranging in size from 1.00-0.420 mm. F: Undeformed muscovite crystals from sample 20D in Colonel Moore Trailhead ranging in size from 1.41-0.420 mm.

kinked muscovite in thin section (Figure 8C). A pelitic sample was provided by Dr. Arthur Snoke. This sample, T5, is a metapelitic rock from a mylonitic shear zone in the northern RMEH. This sample was one subjected to thermobarometric studies by Hodges et al. [1992].

Granite samples from the Harrison Pass Pluton were collected for biotite sampling and did not contain any muscovite. Figure 8 shows samples from the north and west of the Ruby Mountains that have been deformed, with the presence of recrystallized quartz and some muscovite crystals exhibiting kinking in thin section. It also shows undeformed samples from Harrison Pass and Colonel Moore Trailhead in the southeast and east, respectively. These samples do not exhibit deformation because they are farther away from the detachment fault that passes through the western RMEH.

4 ELECTRON MICROPROBE ANALYSIS

4.1 Introduction

Elemental concentrations can be determined through use of electron microprobe analysis (EMPA). This technique utilizes a beam of electrons that is focused onto a thin section sample or grain mount to release characteristic x-rays [*Reed, 2005*]. Energies of the resulting characteristic x-rays can be measured qualitatively using an energy dispersive x-ray detector (EDS) which can be used to identify the minerals. The x-rays can also be measured quantitatively using wavelength dispersive spectrometers (WDS). The WDS permit determination of a chemical analysis of a spot on the sample, typically presented as oxide weight percents for silicate phases.

4.2 Methods

Thin sections were analyzed using the JEOL JXA-8600 Superprobe of Auburn University. This EMPA is equipped with 4 WDS spectrometers, EDS, BSE detectors, and the Geller System upgrade (Figure 9). Thin sections were coated with carbon in a SPI Module Carbon Coater and loaded into the machine. They were analyzed using a 15 kV accelerating voltage and a 20 nA beam current. Elements were calibrated using natural mineral standards (Amelia albite, wollastonite, microcline, anorthite, P-130 garnet, ilmenite, etc.; Table 1). Minerals in the RMEH samples were identified by EDS using the PGT Excalibur program. Samples were then analyzed quantitatively with a 5 micron beam diameter and a 20 second integration time. ZAF matrix corrections used oxide weight percent for major elements to derive oxide weight percentages for use in calculating mineral formulas (see Appendix B).

Figure 9. The JEOL JXA-8600 Superprobe at Auburn University.

Oxide	Crystal	Spectrometer	Standard
SiO2	TAP	2	Amelia Albite
TiO2	PET	3	Ilmenite
Al2O3	TAP	2	Anorthite
FeO	LIF	4	Fayalite
MnO	LIF	4	P-130 Garnet
MgO	TAP	1	Springwater Olivine
CaO	PET	3	Anorthite
Na2O	TAP	1	Amelia Albite
K2O	PET	3	Microcline

Table 1. Elements used in the analysis of micas and the standards on which they were calibrated.

4.3 Results

Tables showing oxide weight percent as well as calculated mineral formulas can be found in Appendix B. Biotite was measured in samples RM8B, RM12, and RM17. Sample RM8B is a pegmatite from Secret Pass, and RM12 and RM17 are a pegmatite and gneiss, respectively, from Lamoille Canyon. Weight percent for FeO was approximately 21-23% for all biotite samples. Calculation of mineral formulas shows this is approximately 60-70% annite and 30-40% phlogopite. Figure 10B shows a graph for the percentages of biotite (annite and siderophyllite) and phlogopite (phlogopite and eastonite).

Muscovite was measured in samples RM8B, RM15, and RM17A. Sample RM15 is a coarse pegmatitic granite from Lamoille Canyon. Weight percent for K_2O was approximately 9-11% for each sample. Calculation of mineral formulas confirm these are indeed samples of muscovite with approximately 95% muscovite and 5% paragonite totals. Figure 10A shows a ternary diagram with the percentages of muscovite depicted.

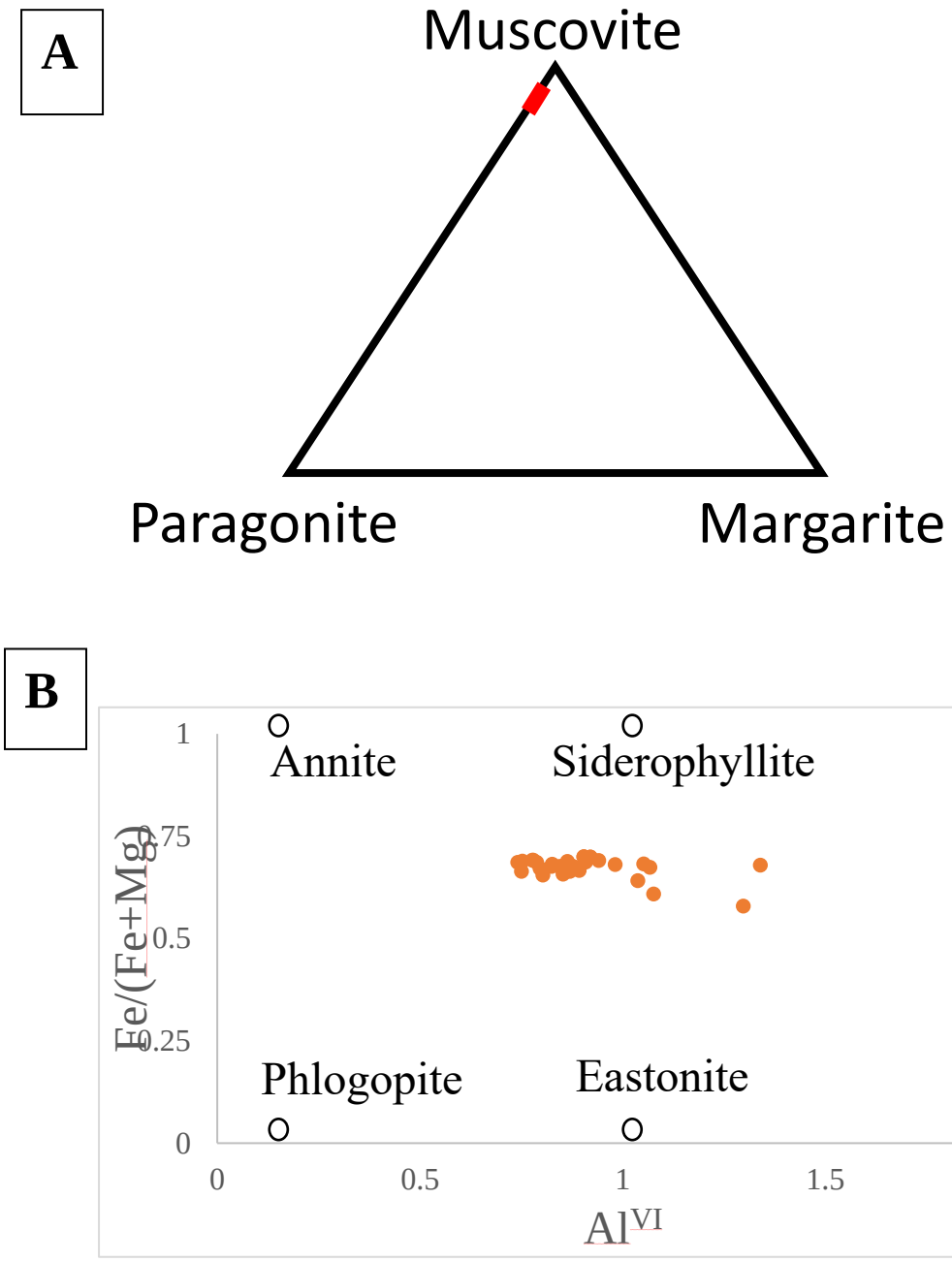

Figure 10. A: Percent muscovite versus paragonite and margarite. B: Percent annite versus phlogopite. Graph modeled after Guidotti [1984].

5 $^{40}Ar/^{39}Ar$ ANALYSIS

5.1 Introduction

Thermal histories of minerals, which can be used to infer crystallization and exhumation histories, can be constrained by determining concentrations of isotopes that are mobile and may be lost by diffusion at high temperature. The first studies of $^{40}Ar/^{39}Ar$ dating were done by Merrihue and Turner [1966], and they pointed out this new method is advantageous over conventional K/Ar methods. This is because measurements can be done at one time on the same sample mass, even single crystals, and absolute abundances are not required. Isotopes of argon that occur naturally include ^{40}Ar, ^{38}Ar, and ^{36}Ar. During age dating, measurements are taken of the abundances of ^{40}Ar, ^{39}Ar, ^{38}Ar, ^{37}Ar, and ^{36}Ar [*McDougall and Harrison,* 1999]. $^{40}Ar^*$ is radiogenic argon formed from decay of ^{40}K, and $^{39}Ar_K$ is produced from ^{39}K during irradiation at a nuclear reactor. The ratio of radiogenic argon given by $^{40}Ar^*/^{39}Ar_K$ is found after using the measurements of ^{36}Ar to make corrections for atmospheric ^{40}Ar. The ratio of these isotopes is used in the calculation of the age using the equation

[1] $$t=1/\lambda*\ln(^{40}Ar/^{39}Ar_K*J+1),$$

where λ represents the decay constant ($5.543x10^{-10}$/year), and J is an irradiation parameter which quantifies the production of $^{39}Ar_K$ during the irradiation process [*Merrihue and Turner,* 1966*;* as summarized by *McDougall and Harrison,* 1999].

Minerals of differing shapes and diameters may develop diffusion gradients with time during cooling, as the argon moves from areas of higher to lower concentration. Diffusion

dimensions can be determined by measuring apparent $^{40}Ar/^{39}Ar$ ages of different spots within single crystals, e.g., from their core to their rims, and indirectly by incremental heating (which tends to sample the edges of diffusion domains first). The relationship between diffusion rate and temperature follow the Arrhenius relationship (as discussed by *McDougall and Harrison* [1999]):

[2] $$D=D_o*\exp(-E/RT)$$

D_o represents the frequency factor, E is the activation energy, and T is the temperature.

The Closure temperature of a mineral is the temperature the sample experienced at the time given by its apparent age [*Dodson,* 1973] Closure temperature can be calculated assuming that variations in grain diameter are the only factor leading to variations in age. Closure temperature, T_c, is defined [*Dodson,* 1973] as

[3] $$T_c=R/[E\mathit{ln}(A\tau D_0/a^2)].$$

R represents the gas constant, A is a geometric constant, a is the diffusion dimension, typically considered as the radius of the grain. The time constant τ is given [*Dodson,* 1973] by

[4] $$\tau=R/(EdT^{-1}/dt)= -RT^2/(EdT/dt)$$

The values for E, D_0, and A have been estimated to be 52 kCal/mol, 0.04 cm^2/s, and 27, respectively, for muscovite [*Hames and Bowring,* 1994]. The values for E, D_0, and A are 47 kCal/mol, 0.04 cm^2/s, and 27, respectively, for biotite [*Harrison et al.,* 1985]. A maximum value for grain radius (a) can be measured directly from the grains in the sample. The minimum grain radius for diffusion cannot be measured readily, since defects may control ^{40}Ar loss and result in a smaller effective grain radius. A smaller effective grain radius of 0.150 mm has been recommended by Harrison et al. [1985] and will be utilized here.

As shown by the relationship in equation 3, larger grains with higher effective diffusion radii ('a') will have higher closure temperatures. Figure 11 depicts how closure temperature works graphically. Figure 11A presents a hypothetical cooling history wherein the slope of the T-t path represents the cooling rate. As a sample cools, K-bearing phases within the rock begin to retain diffusive $^{40}Ar^*$. Retention of ^{40}Ar is expected to begin first in the core of muscovite and biotite crystals. Larger crystals will retain more ^{40}Ar and result in higher ages. As cooling continues and the rims of the crystals begin to retain $^{40}Ar^*$, these crystals become effectively closed. Figure 11B depicts what happens to the daughter to parent ratio ($\sim^{40}Ar^*/^{40}K$) over time. As time increases, the number of $^{40}Ar^*$ atoms retained also increases. This produces the positive trend on the graph. The interval just before the slope becomes linear (red highlight in 11B) is the closure interval for each phase. The Dodson [*1973*] definition of closure temperature essentially extrapolates the closed system (linear) portion of the history to estimate the temperature of the crystal at the time given by its cooling age.

5.2 Methods

Rock samples collected from the Ruby Mountains, Nevada were crushed by hand using a mortar and pestle and sieved through the 14-40 mesh size range (1.4 mm-0.420 mm, respectively). Muscovite crystals were then hand-picked using a binocular microscope (Figure 8) and were loaded into aluminum disks to be sent to the U.S. Geological Survey TRIGA Reactor in Denver, Colorado for neutron irradiation (following procedures outlined by Dalrymple et al. [1981]). In order to monitor the fast neutron flux, samples of monitor minerals with known age were included and interspersed with unknown to detect vertical and radial gradients in J-values. The primary monitor was Fish Canyon sanidine (FC-2, prepared by New Mexico Tech, with an

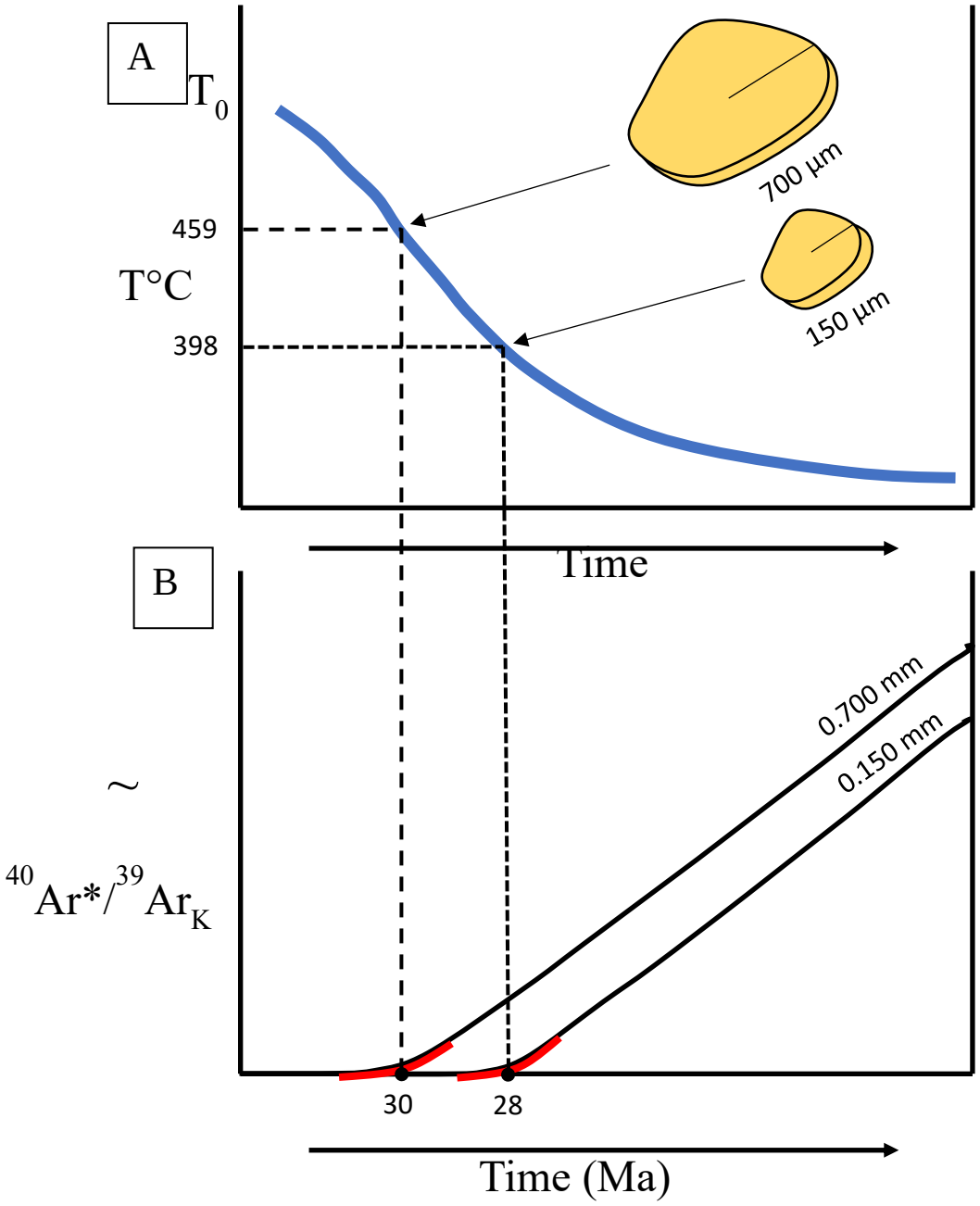

Figure 11. Diagram depicting the concept of closure temperature as discussed in the text. Figure adapted from Dodson, 1973. Two hypothetical crystals are shown, that can be considered to be from the same rock sample and have an identical thermal history, with effective grain radius ('a') of 700 µm and 150 µm, and cooling ages of 30 and 28 Ma, respectively. A: shows a temperature-time path for a sample. B: depicts the ratio of Daughter/Parent isotopes over time. Areas in red represent closure intervals.

assigned age of 28.02 Ma, after Renne et al., 1998), and GA-1550 biotite (prepared by M. Cosca, with an assigned age of 98.09 Ma after Renne et al., 1998). The samples were irradiated with fast neutrons at the central thimble position without Cd shielding for 16 hours.

Upon return, age determinations were completed by fusing single crystals in the Auburn Noble Isotope Mass Analysis Laboratory (ANIMAL) on the GLM-110 spectrometer (Figure 12). The spectrometer is a 10 cm radius, 90 degree sector instrument with double focusing and a single electron multiplier detector. It is automated and run using a Labview program. Single crystals of muscovite were fused by heating for 15 seconds with 12 watts of power from a CO_2 laser, releasing argon isotopes for measurement. Blanks were run following every fifth sample analysis, and air was measured twice daily.

5.3 Results

Muscovite and biotite crystals from rocks in the RMEH yielded intercrystalline (within rock sample) distributions of age with differences of approximately 4 million years. The overall sample to sample age variations is about 12 million years, younging westward toward the Ruby Mountains Detachment fault. These variations result from differences in thermal history and closure temperature. This section will present the age results for each location (also shown in Figures 13-15). For a table of complete results, see Appendix C.

5.3.1 Secret Pass

Muscovite crystals from RM8A and RM9C, two granitic samples from Secret Pass in the northern RMEH, have been dated (Figure 13). The crystals ranged from 1 mm-0.420 mm in diameter. RM8A yielded ages that range from approximately 22.81±0.09 Ma to 21.29±0.04 Ma. Sample RM9C yielded ages ranging from approximately 22.06±0.15 to 21.27±0.02Ma. T5 yielded ages of about 30.46±0.16 to 24.27±0.56 Ma.

Figure 12. A: The new 2000 square foot facility of the Auburn Noble Isotope Mass Analysis Laboratory. B: The GLM-110 in the ANIMAL facility.

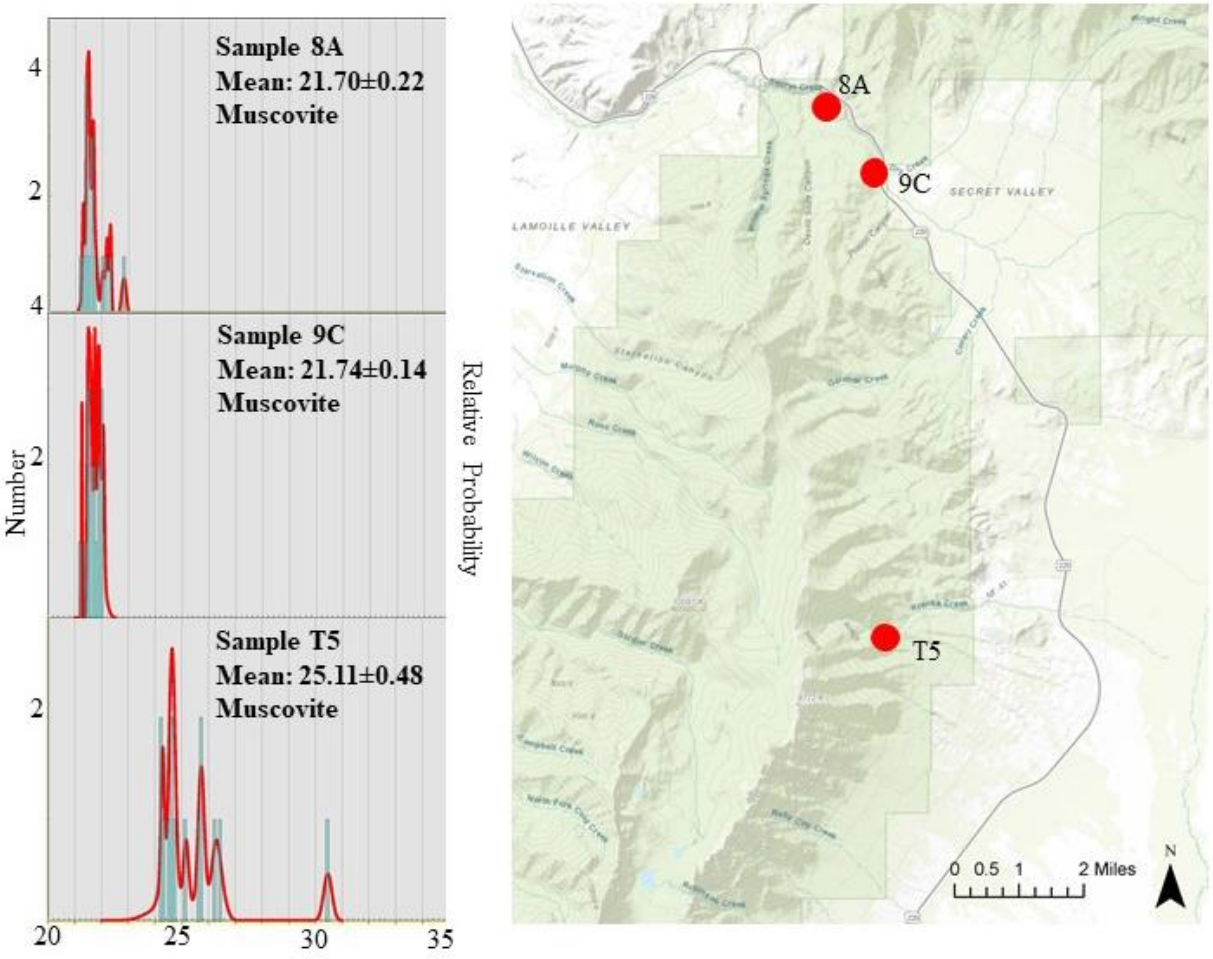

Figure 13. Sample locations and ages of samples RM8A, RM9C, and T5 from Secret Pass in the Northern Ruby Mountains (See Figure 6 for location). Samples RM8A and RM9C were collected in the present study; Sample T5 was collected by Hodges et al., [1992]. Mean ages were calculated using Tukey's biweight mean. This method "ignores the assigned errors of the data points, instead weighting the points according to their scatter from an (iteratively-determined) mean. Points that scatter very far from this 'mean' (whose initial estimate is simply the Median) are de-weighted or even entirely ignored on a sliding scale that depends on the magnitude of their scatter from the 'mean'" [*Ludwig*, 2008]. See Appendix A for additional sample location data.

5.3.2 Lamoille Canyon to Colonel Moore Trailhead

Three samples were collected at the western end of Lamoille Canyon, nearest a normal fault (Figure 14). Muscovite and biotite crystals with diameters ranging from 1 mm-0.420 mm from ten different samples were analyzed. Sample RM15 is a pegmatitic granite from LC with muscovite ages from approximately 25.83±0.04 Ma to 21.26±0.05. RM16A is a sample taken from a fracture face in LC with euhedral quartz and muscovite growth (Figure 7C). The sample yielded muscovite ages ranging from 21.42±0.03 Ma to 20.66±0.07 Ma. Sample 17A is a gneiss from LC with muscovite ages ranging from 21.38±0.07 Ma to 20.79±0.04 Ma. Sample RM12 from LC contained no muscovite, thus biotite ages were determined for RM12. The biotite ages for RM12 were slightly older than the westernmost samples, with a range of 28.22± 0.19 Ma to 25.43±0.05 Ma.

RM21 was collected from Liberty Lake (LL), which is between Lamoille Canyon and Colonel Moore trailhead. Grain diameters for these samples range from 1.40 mm-0.420 mm. This sample yielded ages older than those to the west ranging from 30.04±0.15 Ma to 28.34±0.07 Ma.

The easternmost samples were accessed on public lands in public trail access called the Colonel Moore Trailhead. Widespread and abundant outcrops in the area exposed undeformed muscovite-biotite-granite and pegmatite, with muscovite most suitable for study in pegmatite samples. Samples were selected from each lithology, as shown in Figure 7. These samples include RM19A, RM20C, RM20D, RM20D.2, and RM22. These are all coarse pegmatites with grain diameters ranging from 1 mm-0.420 mm, and larger grain diameters were also measured with RM20D.2 and RM22 (1.68 mm). Muscovite ages for RM19A ranged from 28.68±0.11 Ma to 27.55±0.0.07. RM20C, RM20D, RM20D.2 all yielded similar muscovite ages with ranges of

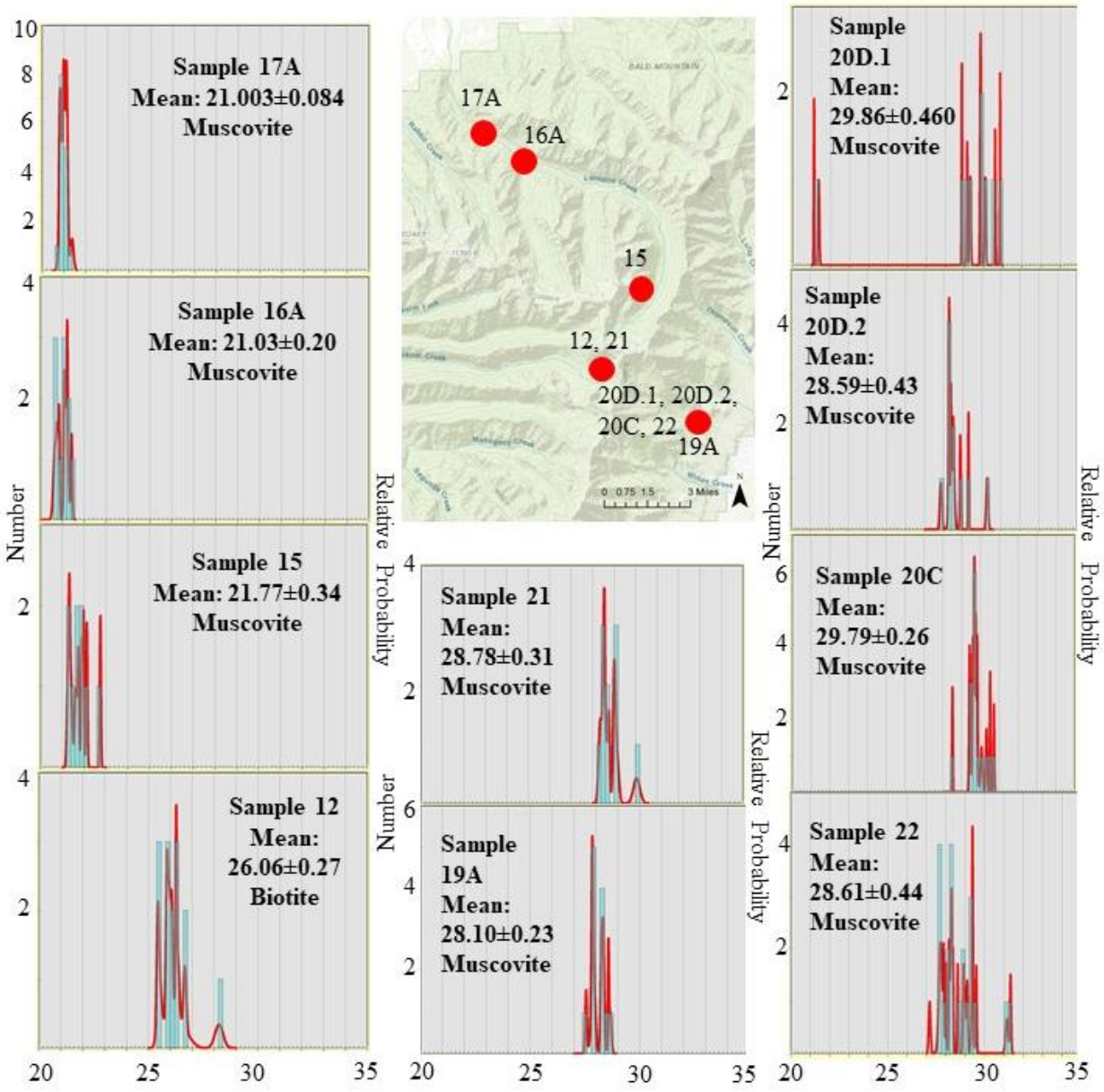

Figure 14. Sample locations and ages of samples RM17A, RM16A, RM15, and RM12 from Lamoille Canyon, RM21 from Liberty Lake, and RM19A, RM20D.1, RM20D.2, RM20C, and RM22 from the Colonel Moore Trailhead area (See Figure 6 for location).

30-28 Ma. Thus, muscovite ages at the eastern side of the Ruby Mountains are ca. 8-10 ma older than ages at the western side at this latitude.

5.3.3 Harrison Pass Pluton

Samples were collected from the Harrison Pass Pluton (HP) in the southern RMEH (Figure 15) with grain diameters ranging from 1.4 mm-0.420 mm. Biotite from two granitic samples, RM4 and RM6, were dated as muscovite was not present. RM4 yielded ages ranging from 36.27±0.14 Ma to 25.04±0.24 Ma. Biotite ages from RM6 ranged from 35.95±0.09 Ma to 35.04±0.1 Ma.

5.3.4 Summary of Ages Determined and Possible Causes for Variation

An overall distribution of ages is shown in figure 16. Samples from this study show a younging trend to the west and the north. All ^{40}Ar samples show variation of age greater than expected by analytical precision, and the most discordance was found in samples RM12 and RM22. Less discordance was found in RM15, RM16, RM17, and the Secret Pass Samples. Variations in mica age, as observed, could arise from differences in closure temperature among single crystals, differences in unsupported ('excess') ^{40}Ar among crystals, or effects of recrystallization or metamorphic fluids. While this study interprets Argon retention and closure to be thermally activated, other studies have suggested retention and closure are affected by the presence of fluids [*Villa and Hanchar*, 2013] or from deformation and recrystallization [*Dunlap,* 1997 and *Cosca et al.*, 2011]. From a lattice diffusion point of view, temperature among mica crystals might be due to variation in D_0 and E (see equation 3), but this seems unlikely as the compositions of muscovite and biotite used are typical of those in previous work to estimate these parameters [*Hames and Bowring,* 1994*; Hames et al.*, 2008*; Harrison et al,* 1985 (biotite)]. Age variations among crystals might also be due to variable incorporation of

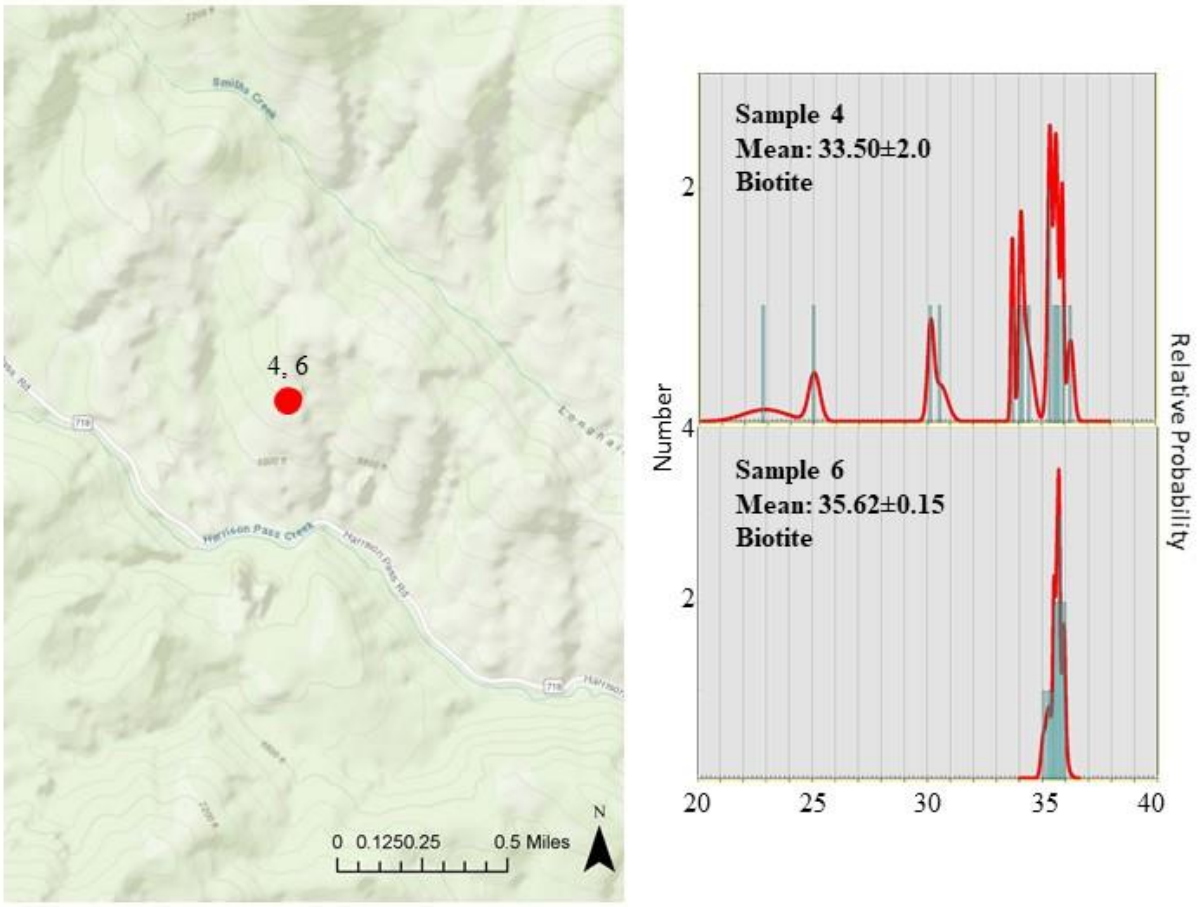

Figure 15. Sample locations and ages of samples RM4 and RM6 from Harrison Pass in the Southern Ruby Mountains (See Figure 6 for location).

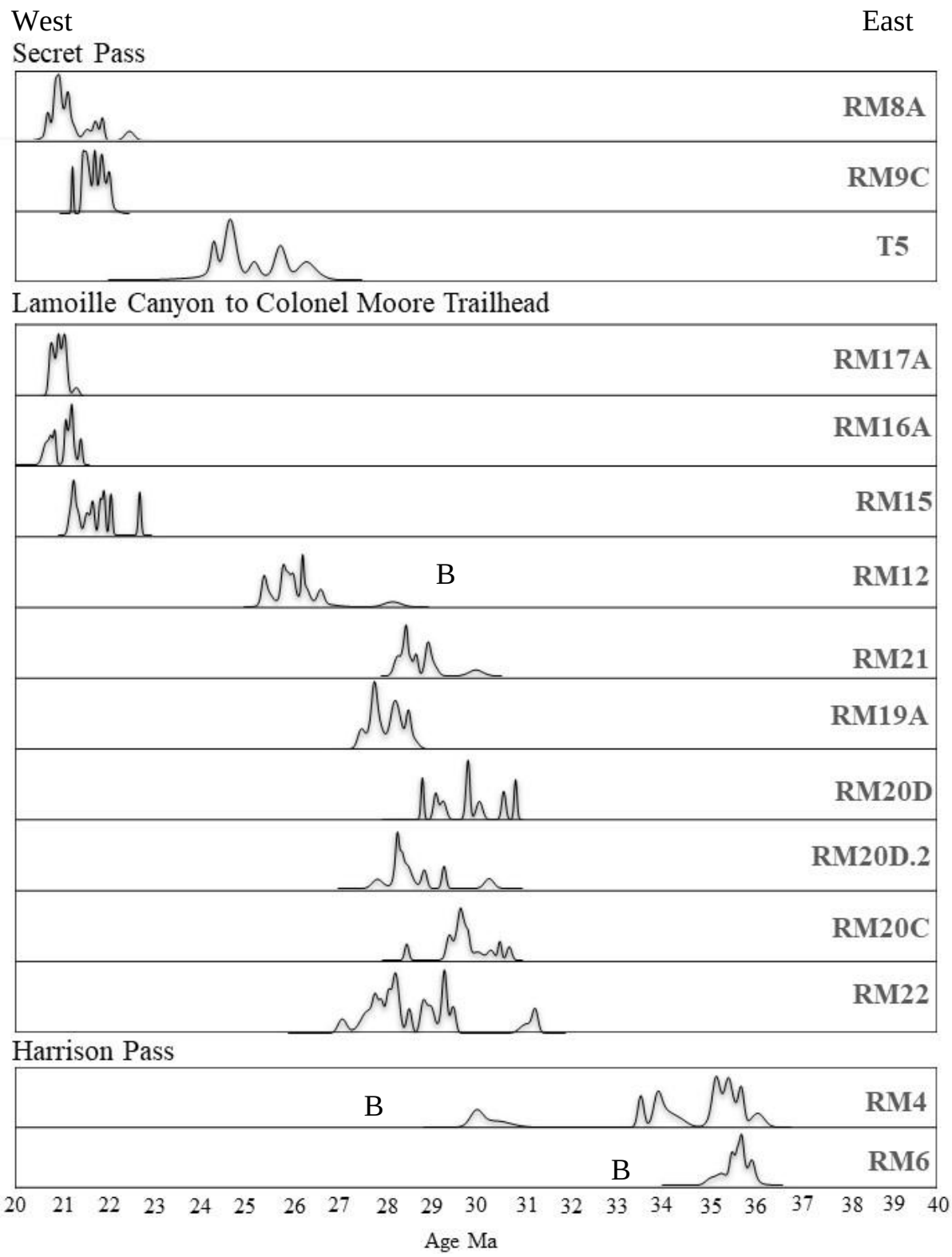

Figure 16. Distribution of ages throughout the RMEH. Samples with 'B' are biotite ages.

unsupported ('excess') ^{40}Ar, but this seems unlikely as the pattern of regional age distribution seems consistent, and muscovite typically does not incorporate excess ^{40}Ar. Variations in intercrystalline age may also arise from grain-to-grain differences in effective diffusion dimension ('a' in equation 3), and this is considered to be a likely cause in consideration of the obvious variations in grain diameter or width (see Figure 8). Variable effects of deformation and recrystallization in micas can also be expected to produce age variations [*Dunlap,* 1997 and *Cosca et al.*, 2011], and likely has a role in some of the observed variations. However, variable loss of $^{40}Ar^*$ during superimposed deformation cannot explain all of the observed age ranges, since some samples were relatively undeformed (e.g. the pegmatitic samples from the Colonel Moore Trailhead area). Thus, for the purposes of the present study, variation in mica $^{40}Ar/^{39}Ar$ ages are interpreted to primarily arise from variations in effective diffusion dimension ('a') and will be modeled accordingly.

6 THERMAL MODELING

6.1 Cooling Rates and Closure Temperature

As previously stated, the closure temperature of a mineral is temperature that a sample experienced at the time given by its apparent age [see equation 2, *Dodson, 1973*]. Inspection of Figure 16 shows that each sample has more variation in age than would be expected from the precision of measurement. Such age range is considered to arise from variations in effective diffusion dimension (500-150 microns for most samples) as discussed previously. Different cooling rates were used iteratively with the maximum and minimum inferred diffusion dimension to produce a calculated range in age that matched the observed. The cooling rate was found to vary by location, and was calculated by subtracting the minimum temperature from the maximum temperature, and dividing it by the intercrystalline age difference. In Secret Pass, the cooling rate was determined to be 30°C/m.y. A Temperature-time graph for samples dated from Secret Pass is shown in Figure 17. A similar rate of approximately 30°C/m.y. was found in Colonel Moore Trailhead and Liberty Lake samples, and a much higher cooling rate of ~75°C/m.y. was calculated in Samples from Lamoille Canyon (Figure 18). In Harrison Pass (figure 19), the cooling rate was approximately 40°C/m.y.-20°C/m.y.

The grain diameter analyzed for most RMEH samples were up to approximately 1.4 mm. For samples RM22 and RM21, larger crystals of muscovite were analyzed, with a maximum diameter of 1.68 mm. Using radii samples for the variables listed above, closure temperatures for RMEH muscovite samples range from 452°C-398°C. The maximum temperature is 459°C for

Figure 17. Temperature-time graph for samples from Secret Pass in the RMEH. The best fit of cooling rates and calculated closure temperatures to the observed range of muscovite ages is compatible with an approximately 30°C/m.y. rate of cooling, as shown.

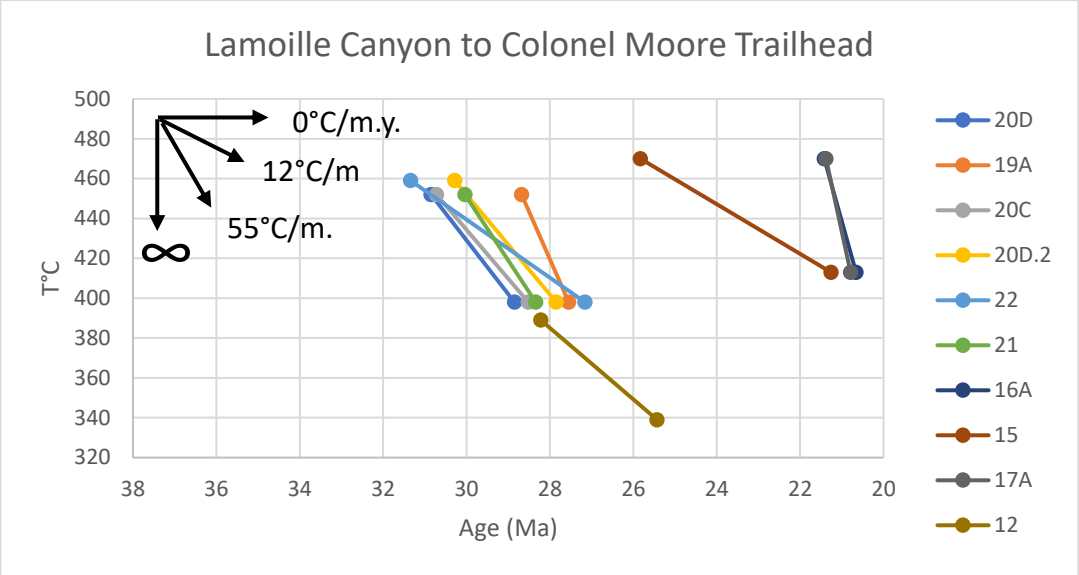

Figure 18. Temperature-time graph for samples from the Lamoille Canyon to Colonel Moore Trailhead transect. The best fit of cooling rates and calculated closure temperatures to the observed range of muscovite ages is compatible with an approximately 30°C/m.y. rate of cooling for the Colonel Moore Trailhead samples. The samples indicate a much higher cooling rate of about 75°C/m.y. for the Lamoille Canyon samples.

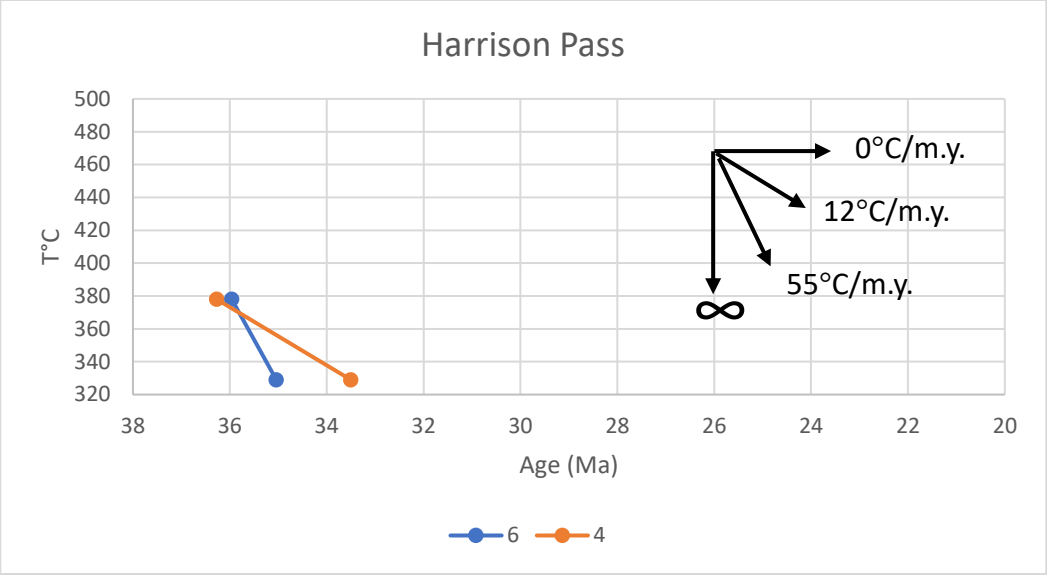

Figure 19. Temperature-time graph for samples from the Harrison Pass. The best fit of cooling rates and calculated closure temperatures to the observed range of biotite ages is compatible with an approximately 40°C/m.y. rate of cooling for RM6 and 20°C/m.y. for RM4, as shown.

sample RM20D.2 and RM22. For the RMEH biotite samples, closure temperature ranges from 389°C-339°C in Lamoille Canyon and 378°C-329°C in Harrison Pass. Closure temperature per sample is reported in Table 2. The closure temperatures varied within samples due to variations in grain diameter. While this concept has been applied in U-Th/He dating methods [*Reiners and Farley*, 2001], it has not been widely used in $^{40}Ar/^{39}Ar$ dating. The findings of this study suggests this method could further be used in $^{40}Ar/^{39}Ar$ dating to yield more accurate results.

Sample #	Max Dimension	Min Dimension	Cooling Rate	*Tc
RM4	0.70 mm	0.15 mm	40°C/m.y.	378-329 °C
RM6	0.70 mm	0.15 mm	20°C/m.y.	366-320 °C
RM8a	0.70 mm	0.15 mm	30°C/m.y.	452-398 °C
RM9c	0.70 mm	0.15 mm	30°C/m.y.	452-398 °C
RM12	0.70 mm	0.15 mm	75°C/m.y.	389-339 °C
RM15	0.70 mm	0.15 mm	75°C/m.y.	470-413 °C
RM16a	0.70 mm	0.15 mm	75°C/m.y.	470-413 °C
RM17a	0.70 mm	0.15 mm	75°C/m.y.	470-413 °C
RM19c	0.70 mm	0.15 mm	30°C/m.y.	452-398 °C
RM20c	0.70 mm	0.15 mm	30°C/m.y.	452-398 °C
RM20d	0.84 mm	0.15 mm	30°C/m.y.	459-398 °C
RM22	0.84 mm	0.15 mm	30°C/m.y.	459-398 °C
RM21	0.70 mm	0.15 mm	30°C/m.y.	452-398 °C

Table 2. Radius range and calculated closure temperature for each sample. Dimension refers to sample radius, and represents the value for '*a*'. Closure temperature varies by approximately 70-90°C between different samples. This is a modeled result of variations in cooling rate among the samples.

7 DISCUSSION

$^{40}Ar/^{39}Ar$ ages of muscovite and biotite from the Ruby Mountains, northeastern Nevada were determined in order to further constrain the pre-Miocene history. The northernmost collected samples include those from Secret Pass (SP) and the sample collected from Dr. Arthur Snoke (T5), which was reported in [*Hodges et al.*, 1992] to have experienced metamorphism during the Cretaceous at depths of approximately 37-39 km. The SP samples are younger with ages ranging from approximately 23-21 Ma. Sample T-5 provided by Dr. Snoke is slightly east of SP, and it yielded older cooling ages of 27-24 Ma after it was exhumed from a depth of approximately 37-39 km at initial equilibration prior to 115 Ma and 13-16 km at final equilibration in the Oligocene. Together, these data indicate rocks from this locale remained at depth until being rapidly exhumed and passing through muscovite closure at around 27-24 Ma. Calculated closure temperatures for the muscovite samples range from 440-398 °C, and these samples are consistent with fairly rapid cooling (Figure 17).

Samples collected from the central transect of the RMEH show a variation in cooling rate from west to the east. (Figure 18). Lamoille Canyon samples were collected from westernmost locations and toward the center, and the Liberty Lake sample was from the center just east and south of Lamoille Canyon. Colonel Moore Trailhead samples were collected from the easternmost location in the RMEH. The oldest ages came from the Colonel Moore Trailhead and Liberty Lake samples and ranged from approximately 31-27 Ma. Samples from Lamoille Canyon were younger with yielded ages of approximately 25-20 Ma and older biotite ages of 28-25 Ma. Ages of muscovite in this transect young to the west with a difference of

approximately 16 million years in age, with faster cooling and exhumation westward. The cooling rates vary from 30°C/m.y. in the east to 75°C/m.y. in the west near the RMEH detachment, as shown on Figure 18. Mean ages were calculated using Tukey's biweight mean. This method "ignores the assigned errors of the data points, instead weighting the points according to their scatter from an (iteratively-determined) mean. Points that scatter very far from this 'mean' (whose initial estimate is simply the Median) are de-weighted or even entirely ignored on a sliding scale that depends on the magnitude of their scatter from the 'mean'" [*Ludwig,* 2008]. An age-distance-elevation plot is shown in Figure 20. This shows a trend of older ages at both higher elevations and further distances from the detachment. Linear regression of the age vs distance data for the transect (using Isoplot 3.70 [*Ludwig*, 2008]) yields a correlation with $R^2 = 0.9561$ and a slope of 0.58±0.10 m.y./km. The slip rate is considered to be the inverse of the slope (after *Foster et al.* [2010]). and calculated to be 1.72 km/m.y., which is faster than nearby Anaconda metamorphic core complex in the northern Rocky Mountains with a reported slip rate of approximately 0.9 km/m.y. at approximately 53-39 Ma [*Foster et al.*, 2010]. However, this rate is slower than the Harcuvar and Buckskin Mountains in Arizona with a reported slip rate of 7-8 km/m.y. between 21-14 Ma [*Foster et al.*, 1993]. A similar slip rate of approximately 1 km/m.y. during early to mid-Miocene was reported for the northern Snake Range in eastern Nevada [*Lee et al.,* 2017].

The Harrison Pass (HP) pluton is located in the southern Ruby Mountains. Biotite ages were reported from the HP pluton by Colgan et al. [2010]. Along with ages, they also mapped biotite age contours (see figure 6). Biotite crystals from samples collected in phases of the HP pluton yielded the oldest ages of around 36 to 35 Ma. With calculated closure temperatures showing $^{40}Ar^*$ retention from approximately 367-329 °C, sample RM4 and sample RM6 indicate

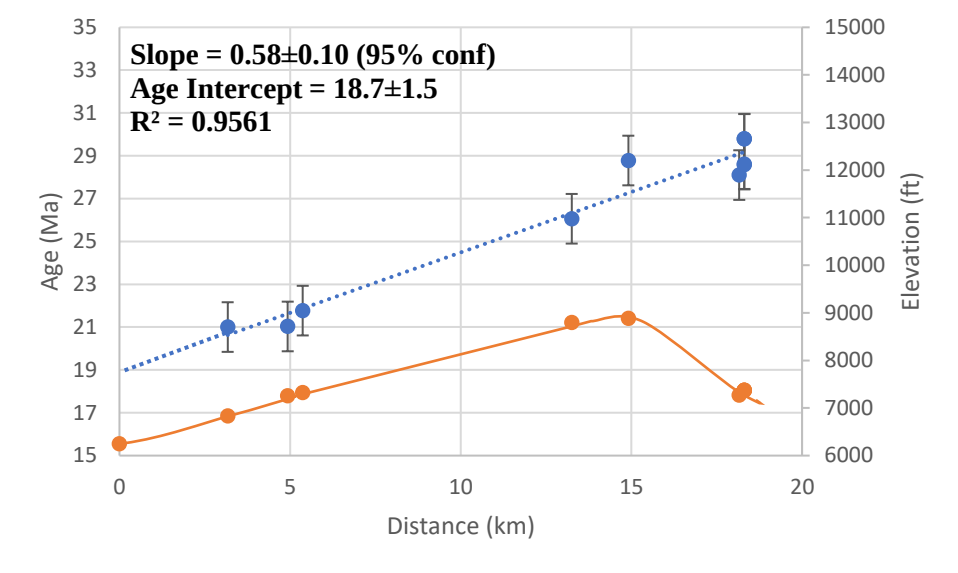

Figure 20. Age-Distance-Elevation plot for samples along the central transect with distance increasing to the east away from the detachment. The mean ages represented in this figure are based on data presented in Figures 13-15.

cooling rates of 40°C/m.y. to 20°C/m.y. (Figure 19). Biotite from Harrison Pass was previously studied by Colgan et al [2010], who reported biotite age contours. The HP samples from this study are consistent with the age contours that Colgan et al. [2010] mapped from their biotite data. All other samples in the present study support the age contours of Colgan et al. [2010] with the exception of some biotite samples which are found to have ages of older than 30 Ma (see Figure 6).

The ages from the RMEH samples range from approximately 20 Ma to 36 Ma. This 16-million-year difference is significant, as it indicates that west to east extension in the RMEH began by the Late Eocene and continued through the Oligocene and into the Miocene. Samples from the northern RMEH reached final equilibrium at temperatures of approximately 646-546°C [*Hodges et al., 1992*] before they were unroofed and passed through muscovite closure at approximately 23-21 Ma. Data of the present study are consistent with the suggestion by Hodges et al. [*1992*] that much of the extension and exhumation of the RMEH may be pre-Tertiary.

The Basin and Range province, including the area of northeastern Nevada that contains the RMEH, experienced crustal thickening from thrusting during the Jurassic into the Cretaceous [*Coney and Harms,* 1984*; DeCelles,* 2004] and later underwent extension and exhumation events that exposed deep crustal rocks. The data suggest that the RMEH underwent extension constantly over a period of almost 20 million years, with possible bursts of rapid episodes with rates of uplift of approximately 30°C/m.y. around 28-30 Ma resulting in the exposure of rocks in the eastern RMEH, and approximately 75°C/m.y. around 19-21 Ma resulting in the exposure of rocks in the western RMEH (Figure 16). Figure 21 depicts the evolution of the detachment fault of the RMEH metamorphic core complex over this time. Though the cooling rate for the western RMEH seems high, it is supported as the pegmatites yield zicon ages of approximately 29 Ma, as

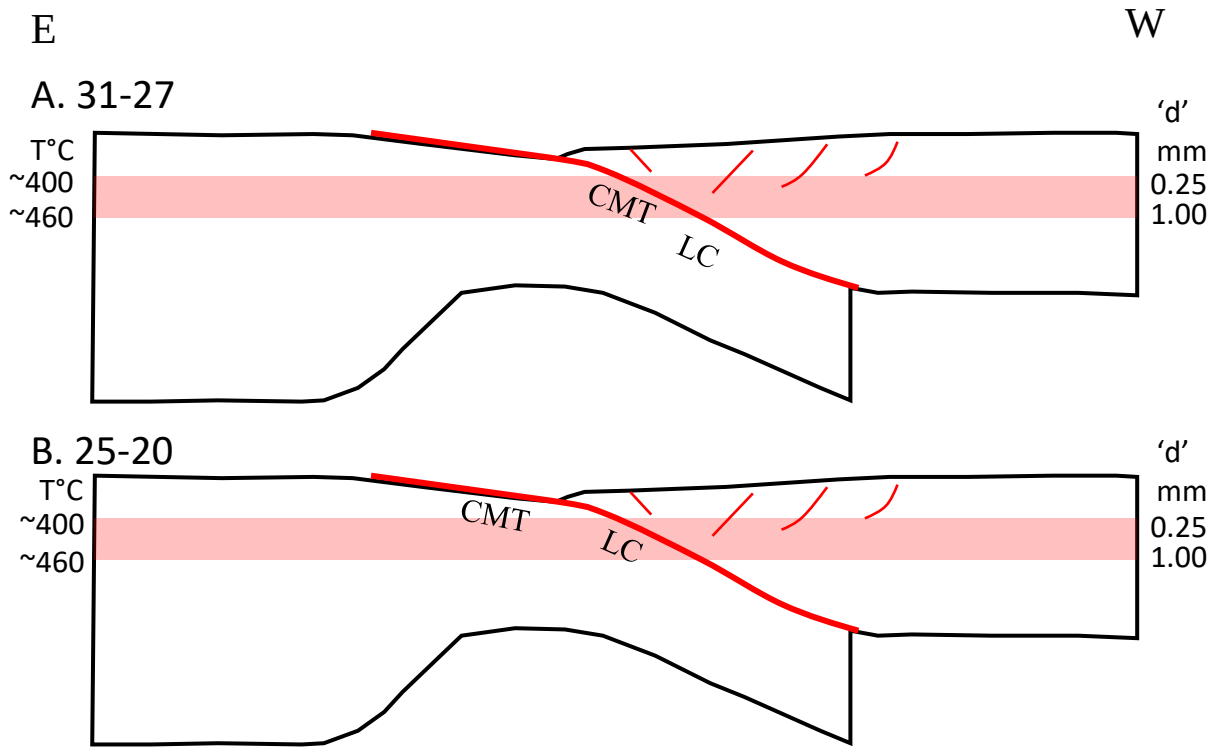

Figure 21. Evolution of the RMEH metamorphic core complex detachment fault, viewed from the north. The bold red line represents the fault, and the shaded red area represents the muscovite closure interval. Exhumation of crust thickened during Sevier orogeny through muscovite closure began by ~31 Ma, and was complete by 19 Ma. Rocks east of Lamoille Canyon (Colonel Moore Trailhead) cooled through muscovite closure at 30°C/m.y. in the Oligocene. Extension accelerated by the early Miocene, accompanied by cooling at up to 75°C/Ma, for rocks at the west end of Lamoille Canyon and immediately beneath the Ruby Mountains detachment fault. Figure adapted from *Platt et al.* [2015].

discussed previously [*Wright and Snoke,* 1993*; Howard et al.,* 2011]. For muscovite ages to be approximately 22-20 Ma, the rocks would have to be cooling rapidly through higher temperatures to reach muscovite closure from zircon closure within 7 Ma, as zircon could be expected to retain lead during growth in the pegmatite-forming melt at approximately 850°C. As most of the data in the present study are from pegmatites, it could seem that the rapid cooling might only reflect pegmatite intrusion into relatively cool country rock. However, sample T-5, from a metamorphic assemblage, yields ages consistent with rapid cooling. Thus rapid cooling and generation of Oligocene to Miocene pegmatite appear to have occurred in the same tectonic episode. From the data of the present study along with the major late Miocene extensional episode presented by Colgan and Henry [2009], one can interpret that the RMEH underwent constant extension beginning in the Eocene that continued and possibly accelerated into the Miocene. Figure 22 shows the closure temperature and age of all the data as modeled in this study. As shown by the graph, the samples from different locations within the RMEH cooled at variable rates at different points in time, with an age range of 16 million years between them. The graph shows a clear trend of ages of samples younging to the northwest, indicating samples to the southeast were exhumed before samples toward the northwest.

The present study utilized a novel way to interpret $^{40}Ar/^{39}Ar$ cooling age data and constrain temperature-time histories, as it assumes variations in grain diameter are the only factor leading to variations in intercrystalline ages of a given sample. Alexandre [2011] used a similar approach in studies of slowly cooled Proterozoic lithologies. In that study, Alexandre found approximately 273 million years of plateau age variation for bulk samples among grain sizes he modeled as ranging from 63-1000 μm. In his study, samples were crushed using a jaw crusher. In the present study, samples were crushed by hammer which more efficiently eliminates grain

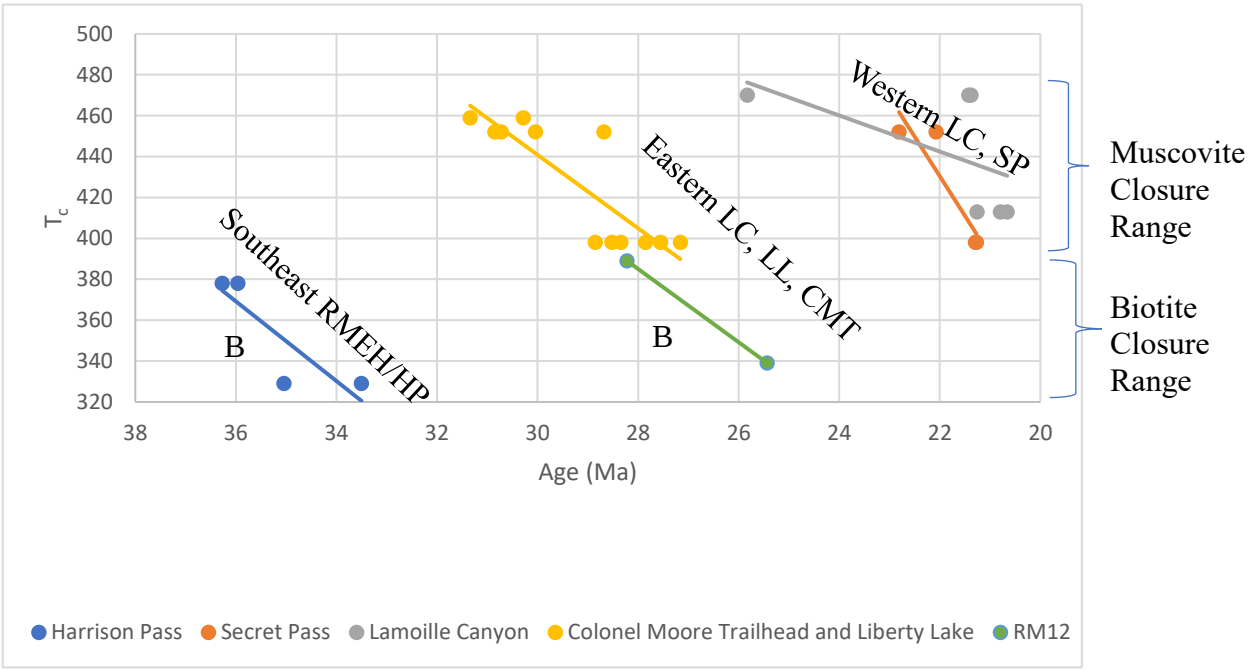

Figure 22. Closure temperature vs time graph for age data in the Ruby Mountains. Biotite results for Lamoille Canyon and Harrison Pass are shown with 'B;' all others are muscovite. Abbreviations: RMEH – Ruby Mountains East Humboldt range, LC- Lamoille Canon, LL- Liberty Lake, CMT- Colonel Moore Trailhead, SP- Secret Pass.

breakage. This study also utilized single crystal fusion which can constrain intercrystalline as well as intracrystalline ages. The present study also demonstrates age variations among coexisting mica crystals in a rapidly cooled Miocene terrane. Thus, the phenomenon of grain-size dependent closure is not restricted to old and slowly cooled terrains.

8 CONCLUSION

Previous work indicates the Ruby Mountains East Humboldt (RMEH) metamorphic core complex underwent multiple stages of uplift from the Cretaceous to the Late Miocene. New data of the present study show that overthickened crust of the RMEH was uplifted from beneath a westward dipping detachment to produce closure for ^{40}Ar diffusion in micas from the Eocene into the early Miocene. Retention of 40Ar* in micas began by ca. 36 Ma to the east and south, then progressed northwestward to final closure of 40Ar* in micas by ca. 20 Ma in the western Lamoille Canyon and Secret Pass areas. The rates of cooling were not consistent over time with rates of approximately 30°C/m.y. close to 30 Ma in southeastern locales and appears to have accelerated up to 75°C/m.y. around 20 Ma in northwestern locales. This acceleration could have continued through the Miocene, however, the new data from this study show that mid-crustal uplift (with attendant retention of ^{40}Ar in micas) and extension along the RMEH detachment fault began by the Oligocene and was complete prior to upwelling of the Yellowstone hotspot at approximately 17 Ma. The calculated average slip rate in the central RMEH range of the present study is comparable to other metamorphic core complexes in the broader Basin and Range province. As Colgan et al. [2010] calculated a slip rate for the Ruby detachment of 2-4 and 3-6 km/m.y. at 17-16 Ma, the present calculations of 1.72 km/m.y. from approximately 30-20 Ma could be interpreted to reflect an acceleration of slip rate in the middle Miocene.

The methods used in the present study show promise for interpreting ^{40}Ar/^{39}Ar cooling ages for single crystals of micas. The model that the effective diffusion radius (‘a’) is a function of physical grain size, and a choice of a=700 to 150 μm in this study leads to regional patterns of

cooling rates and closure temperatures that are sensible from a tectonic point of view and from postulated diffusion parameters for micas. The use of single crystal ages, as in this study, has the potential for yielding more useful and accurate constraints to a cooling history than could be obtained from bulk-sample methods of age dating.

REFERENCES

Alexandre, P. (2011) Comparison between grain size and multi-mineral 40Ar/39Ar thermochronology, Geochimica et Cosmochimica Acta, 75, 4260-4272.

Armstrong, R.E., P. Ward (1991), Evolving geographic patterns of Cenozoic magmatism in the North American Cordillera: the temporal and spatial association of magmatism and metamorphic core complexes, Journal of Geophysical Research, 96(B8), 13201-13224.

Brueseke, M.E., M.T. Heizler, W.K. Hart, S.A. Mertzman (2007) Distribution and geochronology of Oregon Plateau (U.S.A.) flood basalt volcanism: The Steens Basalt revisited, Journal of Volcanology and Geothermal Research, 161, 187–214.

Camp, V.E., K.L. Pierce, and L.A. Morgan (2015) Yellowstone plume trigger for Basin and Range extension, and coeval emplacement of the Nevada–Columbia Basin magmatic belt, Geosphere, 11(2), 1-23, doi: 10.1130/GES01051.1.

Colgan, J.P., and C.D. Henry (2009) Rapid middle Miocene collapse of the Mesozoic orogenic plateau in northcentral Nevada: International Geology Review, 51(9–11), 920–961.

Colgan, J.P., K.A. Howard, R.J. Fleck, and J.L. Wooden (2010), Rapid middle Miocene extension and unroofing of the southern Ruby Mountains, Nevada, Tectonics, 29, 1-38, doi:10.1029/2009TC002655.

Coney, P.J. and T.A. Harms (1984) Cordilleran metamorphic core complexes: Cenozoic extensional relics of Mesozoic compression, Geology, 12, 550-554.

Cosca, M., H. Stunitz , A.-L. Bourgeix , and J.P. Lee (2011) 40Ar* loss in experimentally deformed muscovite and biotite with implications for 40Ar/39Ar geochronology of naturally deformed rocks, Geochimica et Cosmochimica Acta, 75(24), 7759-7778.

Dallmeyer, R.D., A.W. Snoke, E.H. McKee (1986) The Mesozoic-Cenozoic tectonothermal evolution of the Ruby Mountains, East Humboldt Range, Nevada: a Cordilleran metamorphic core complex, Tectonics, 5(6), 931-954.

Dalrymple, G.B., E.C. Alexander, M.A. Lanphere, and G.P. Kraker, (1981), Irradiation of samples for 40Ar/39Ar dating using the Geological Survey TRIGA Reactor, Geological Survey Professional Paper, 1176, 1-55.

DeCelles, P.G. (2004), Late Jurassic to Eocene evolution of the Cordilleran thrust belt and foreland basin system, western U.S.A., American Journal of Science, 304, 105-168.

Dewey, J.F., and J.M. Bird (1970) Mountain Belts and New Global Tectonics, Journal of Geophysical Research, 75(14), 2625-2647.

Dewey, J.F. (1988) Extensional Collapse of Orogens, Tectonics, 7(6), 1123-1139.

Dodson, M.H. (1973) Closure temperature in cooling geochronological and petrological systems, Contributions to mineralogy and petrology, 40(3), 259-274.

Dokka R.K., M.J. Mahaffie, and A.W. Snoke (1986) Thermochronologic evidence of major tectonic denudation associated with detachment faulting, northern Ruby Mountains- East Humboldt Range, Nevada, Tectonics 5(7), 995-1006.

Dunlap, W.J., (1997) Neocrystallization or cooling? $^{40}Ar/^{39}Ar$ ages of white micas from low-grade mylonites, Chemical Geology, 143, 181-203.

Eaton, G.P (1982) The Basin and Range Province: Origin and Tectonic Significance, Ann. Rev. Earth Planet. Sci., 10, 409-440.

England, P. C. (1982) Some numerical investigations of large scale continental deformation. In Hsu¨ , K. J., ed. Mountain building processes. New York, Academic Press, 129–139.

Foster, D.A., A.J.W. Gleadow, S.J. Reynolds, and P.G. Fitzgerald (1993) Denudation of Metamorphic Core Complexes and the Reconstruction of the Transition Zone, West Central Arizona, Constraints From Apatite Fission Track Thermochronology, Journal of Geophysical Research, 98, 2167-2185.

Foster, D.A., W.C. Grice Jr., and T.J. Kalakay (2010) Extension of the Anaconda metamorphic core complex: 40Ar/39Ar thermochronology and implications for Eocene tectonics of the northern Rocky Mountains and the Boulder batholith, Lithosphere, 2(4), 232-246.

Guidotti, C. (1984) Micas in Metamorphic Rocks, Reviews in Mineralogy and Geochemistry, 13(1), 357-467.

Haines, S.H., and B.A. Van Der Pluijm (2010) Dating the detachment fault system of the Ruby Mountains, Nevada: Significance for the kinematics of low-angle normal faults, Tectonics, 29, 1-20, doi:10.1029/2009TC002552.

Hames, W.E. and S.A. Bowring (1994) An empirical evaluation of the argon diffusion geometry in muscovite, Earth and Planetary Science Letters, 124, 161-167.

Hames, W., D. Unger, J. Saunders, and G. Kamenov (2009) Early Yellowstone hotspot magmatism and gold metallogeny, Journal of Volcanology and Geothermal Research, 188, 214-224.15.

Hames, W.E., J.T. Cheney, and R.J. Tracy (2008) Single-crystal Ar-40/Ar-39 age variation in muscovite of the Gassetts Schist and associated gneiss, Vermont Appalachians, American Mineralogist, 93(2-3), 384-395.

Harrison, T.M., I. Duncan, and I. McDougall (1985) Diffusion of 40Ar in biotite: Temperature, pressure and compositional effects, Geochemica et Cosmochimica Acta, 49, 2461-2468.

Hodges, K.V., A.W. Snoke, and H.A. Hurlow (1992) Thermal evolution of a portion of the Sevier Hinterland: the northern Ruby Mountains-East Humboldt range and Wood Hills, northeastern Nevada, Tectonics, 11(1), 154-164.

Howard, K.A., J.L. Wooden, C.G. Barnes, W.R. Premo, A.W. Snoke, and S.-Y. Lee (2011) Episodic growth of a Late Cretaceous and Paleogene intrusive complex of pegmatitic leucogranite, Ruby Mountains core complex, Nevada, USA, Geosphere, 7(5), 1220-1248, doi: 10.1130/GES00668.1.

John, D.A. (2001) Miocene and early Pliocene epithermal gold-silver deposits in the northern Great Basin, western United States: characteristics, distribution, and relationship to magmatism, Economic Geology, 96, 1827-1853.

Kistler, R.W., E.D. Ghent, and J.R. O'Neil (1981) Petrogenesis of Garnet Two-Mica Granites in the Ruby Mountains, Nevada, Journal of Geophysical Research, 86(B11), 10591-10606.

Lee, J., T. Blackburn, and S. Johnston (2017) Timing of mid-crustal ductile extension in the northern Snake Range metamorphic core complex, Nevada: Evidence from U/Pb zircon ages, Geosphere, 13(2), 439-459.

Ludwig, K.R. (2008) User's manual for Isoplot, v. 3.0, a geochronological toolkit for Microsoft Excel, Berkeley Geochronological Center, Special Publication no. 4.

Lund Snee, J.E., E.L. Miller, M. Grove, J.K. Hourigan, and A. Konstantinou (2016) Cenozoic paleogeographic evolution of the Elko Basin and surrounding region, northeast Nevada, Geosphere, 12(2), 464-500, doi: 10 .1130 /GES01198.1.

MacCready T., A.W. Snoke, J.E. Wright, and K.A. Howard (1997) Mid-crustal flow during Tertiary extension in the Ruby Mountains core complex, Nevada, GSA Bulletin, 109(12), 1576-1594.

McDougall, I., and T. M. Harrison (1999), Geochronology and Thermochronology by the 40Ar/39Ar Method, 2nd ed., 269 pp., Oxford Univ. Press, New York.

McGrew, A.J. and L.W. Snee (1994) $^{40}Ar/^{39}Ar$ thermochronologic constraints on the tectonothermal evolution of the northern East Humboldt Range metamorphic core complex, Nevada, Tectonophysics 238, 425-450.

Merrihue, C. and G. Turner (1966) Potassium-Argon dating by activation with fast neutrons, Journal of Geophysical Research, 71(11), 2852-2857.

Parsons, T, G.A. Thompson, and N.H. Sleep (1994), Mantle plume influence on the Neogene uplift and extension of the U.S. western Cordillera?, Geology, 22, 83-86.

Pierce, K.L. and L.A. Morgan (1992), The track of the Yellowstone hot spot: Volcanism, faulting, and uplift, Geological Society of America Memoirs, 179.

Platt, J.P., Behr, W.M., and F.J. Cooper (2015) Metamorphic core complexes: windows into the mechanics and rheology of the crust, Journal of the Geological Society, 172, 9-27.

Reed, S.J.B. (2005), Electron Microprobe Analysis and Scanning Electron Microscopy in Geology, 1st ed., Cambridge University Press, New York.

Renne, P.R., C.C. Swisher, A.L. Deino, D.B. Karner, T.L. Owens, and D.J. DePaolo, (1998), Intercalibration of standards, absolute ages and uncertainties in 40Ar/39Ar dating, Chemical Geology, 145, 117-152.

Reiners, P.W. and K.A. Farley (2001) In£uence of crystal size on apatite (U^Th)/He thermochronology: an example from the Bighorn Mountains, Wyoming, Earth and Planetary Science Letters, 188, 413-420.

Saltus, R.W. and G.A. Thompson (1995), Why is it downhill from Tonopah to Las Vegas?: A case for mantle plume support of the high northern Basin and Range, Tectonics, 14, 1235-1244.

Snell, K.E., P.L. Koch, P. Druschke, B.Z. Foreman, and J.M. Eiler (2014) High elevation of the 'Nevadaplano' during the Late Cretaceous, Earth and Planetary Science Letters, 386, 52-63.

Snoke, A. W., and D. M. Miller (1988), Metamorphic and tectonic history of the northeastern Great Basin, in Metamorphism and Crustal Evolution of the Western United States, Rubey Volume VII, edited by W. G. Ernst, pp. 606–648, Prentice Hall, Englewood Cliffs, N. J.

University of Utah, Yellowstone Hotspot Overview, The Yellowstone-Teton Epicenter, http://www.yellowstonegis.utah.edu/research/hotspot.html

Villa, I. and J. Hanchar (2013). K-feldspar hygrochronology. Geochimica et Cosmochimica Acta. 101. 24-33.

Wright, J. E., and A. W. Snoke (1993), Tertiary magmatism and mylonitization in the Ruby-East Humboldt metamorphic core complex, Northeastern Nevada: U-Pb geochronology and Sr, Nd, and Pb isotope geochemistry, Geol. Soc. Am. Bull., 105, 935–952.

APPENDIX A: SAMPLE INFORMATION

Sample #	Rock Type	Latitude	Longitude	Location	Phases Picked	Grain size (μm)	Elevation (ft)
RM4	Granodiorite	40 18’32.5”N	115 28’17.4”W	Harrison Pass	biotite	1400-300	6510
RM6	granite	40 18’ 57.1”N	115 29’21.2”W	Harrison Pass	biotite	1400-300	6645
RM8a	Deformed felsic (chips)	40 51’35.1”N	115 14’07.3”W	Secret Pass	muscovite	1400-300	6335
RM9c	chips of deformed granite &gneiss	42 51’11.2”N	117 12’45.4”W	Secret Pass	muscovite	1400-300	6427
RM12	pegmatite	40 36’19.3”N	115 22’33.5”W	Lamoille Canyon	biotite	1400-300	8798
RM15	coarse pegmatitic granite	40 39’36.3”N	115 26'11.0”W	Lamoille Canyon	muscovite	1400-300	7324
RM16a	face of fracture surface	41 39’36.3”N	116 26'11.0”W	Lamoille Canyon	muscovite	1400-300	7260
RM17a	gneiss	40 40’25.9”N	115 27'50.0”W	Lamoille Canyon	muscovite	1400-300	6834
RM19c	musc/qtz vein	40 33’44.0”N	115 21'13.9”W	Colonel Moore Trailhead	muscovite	1400-300	7269
RM20c	granite	42 33’47.8”N	117 21'14.7”W	Colonel Moore Trailhead	muscovite	1400-300	7369
RM20d	books of muscovite from pegmatite	43 33’47.8”N	118 21'14.7”W	Colonel Moore Trailhead	muscovite	1680-300	7369
RM22	undeformed granite	44 33’47.8”N	119 21'14.7”W	Colonel Moore Trailhead	muscovite	1680-300	7369
RM21	granite	40 35'44.3"N	115 22'33.4"W	Liberty Lake	muscovite	1400-300	8883
T-5	garnet muscovite schist	40 45'N	115 15'W	Northern RMEH	muscovite	1400-300	9263

Sample T-5 is from Hodges et al. [1992]. Latitude and Longitude coordinates are estimated from Figure 1 in Hodges et al. [1992].

APPENDIX B: EMPA DATA

RM15 Muscovite, Electron microprobe analyses												
Oxide Wt%	**42**	**43**	**44**	**45**	**46**	**47**	**48**	**49**	**50**	**51**	**52**	**12**
SiO2	44.55	43.26	43.13	44.06	45.89	45.85	46.08	45.72	46.03	52.43	45.57	0.54
TiO2	0.80	0.77	0.89	0.58	0.63	0.69	0.61	0.61	0.58	0.98	0.08	0.55
Al2O3	35.01	34.83	34.89	34.76	35.68	35.68	35.78	35.61	35.88	28.76	29.92	35.60
FeO	1.88	2.03	1.78	1.93	1.98	1.87	1.83	1.82	1.84	3.26	9.82	45.32
MnO	0.00	0.02	0.01	0.02	0.02	0.01	0.04	0.00	0.03	0.04	0.03	11.06
MgO	0.53	0.54	0.54	0.50	0.61	0.56	0.52	0.52	0.54	1.20	1.28	0.02
CaO	0.03	0.00	0.01	0.01	0.01	0.02	0.00	0.00	0.01	0.20	0.22	1.91
Na2O	0.41	0.48	0.48	0.55	0.53	0.60	0.51	0.61	0.52	0.00	0.16	0.00
K2O	10.80	10.91	10.94	10.99	11.22	11.04	11.13	10.90	11.13	9.80	7.93	0.59
Total	94.00	92.84	92.67	93.39	96.56	96.33	96.49	95.80	96.55	96.68	95.01	95.58
Cations (on the basis of 22 O)												
Si	6.05	5.98	5.97	6.04	6.08	6.08	6.10	6.09	6.09	6.86	6.28	0.10
Ti	0.08	0.08	0.09	0.06	0.06	0.07	0.06	0.06	0.06	0.10	0.01	0.08
AlIV	1.95	2.02	2.03	1.96	1.92	1.92	1.90	1.91	1.91	1.14	1.72	7.90
AlVI	3.66	3.65	3.65	3.66	3.65	3.66	3.68	3.68	3.68	3.29	3.13	0.16
Fe	0.21	0.23	0.21	0.22	0.22	0.21	0.20	0.20	0.20	0.36	1.13	7.28
Mn	0.00	0.00	0.00	0.00	0.00	0.00	0.00	0.00	0.00	0.00	0.00	1.80
Mg	0.11	0.11	0.11	0.10	0.12	0.11	0.10	0.10	0.11	0.23	0.26	0.00
Ca	0.00	0.00	0.00	0.00	0.00	0.00	0.00	0.00	0.00	0.03	0.03	0.39
Na	0.11	0.13	0.13	0.15	0.14	0.15	0.13	0.16	0.13	0.00	0.04	0.00
K	1.87	1.92	1.93	1.92	1.90	1.87	1.88	1.85	1.88	1.64	1.39	0.15
IV	8.00	8.00	8.00	8.00	8.00	8.00	8.00	8.00	8.00	8.00	8.00	8.00
VI	4.07	4.08	4.07	4.05	4.06	4.05	4.05	4.05	4.05	3.98	4.54	9.32
Sum Alk.	1.98	2.05	2.06	2.07	2.03	2.03	2.01	2.01	2.01	1.66	1.47	0.54
%Mus	0.94	0.94	0.94	0.93	0.93	0.92	0.94	0.92	0.93	0.98	0.95	0.27
%par	0.05	0.06	0.06	0.07	0.07	0.08	0.06	0.08	0.07	0.00	0.03	0.00
%Mar	0.00	0.00	0.00	0.00	0.00	0.00	0.00	0.00	0.00	0.02	0.02	0.73

RM8B Muscovite, Electron microprobe analyses											
Oxide Wt%	**22**	**23**	**1**	**2**	**3**	**4**	**5**	**6**	**7**	**8**	**9**
SiO2	43.71	44.69	44.91	43.79	44.82	45.34	45.83	45.99	45.23	46.55	46.09
TiO2	0.3498	0.6213	0.5103	0.3217	0.3993	0.6685	0.4765	0.3243	0.543	0.2577	0.3048
Al2O3	34.58	34.49	35.38	34.69	35.66	34.13	35.06	34.8	34.99	36.27	35.16
FeO	1.2774	1.3061	1.4947	1.5046	1.2849	1.5801	1.5763	1.6394	1.6764	1.4708	1.1216
MnO	0.0443	0.0284	0.0289	0.0414	0	0.0585	0	0	0.0042	0.0584	0
MgO	0.2761	0.7059	0.509	0.5037	0.4613	0.6256	0.6482	0.7143	0.527	0.5869	0.5087
CaO	0.0432	0.0085	0.0037	0	0	0	0.0261	0.0473	0.0149	0.0187	0.0708
Na2O	0.3977	0.4064	0.3211	0.4067	0.5581	0.3714	0.2983	0.3644	0.3962	0.298	0.2679
K2O	11.69	11.45	11.83	11.58	11.79	11.9	12.21	11.9	11.86	12.22	11.98
Total	92.36	93.7	94.98	92.83	94.97	94.68	96.12	95.79	95.25	97.73	95.51
Cations (on the basis of 22 O)											
SiO2	6.07	6.10	6.06	6.05	6.05	6.15	6.12	6.15	6.09	6.10	6.16
TiO2	0.04	0.06	0.05	0.03	0.04	0.07	0.05	0.03	0.06	0.03	0.03
AlIV	1.93	1.90	1.94	1.95	1.95	1.85	1.88	1.85	1.91	1.90	1.84
AlVI	3.72	3.65	3.69	3.70	3.71	3.60	3.64	3.64	3.65	3.70	3.71
FeO	0.15	0.15	0.17	0.17	0.14	0.18	0.18	0.18	0.19	0.16	0.13
MnO	0.01	0.00	0.00	0.00	0.00	0.01	0.00	0.00	0.00	0.01	0.00
MgO	0.06	0.14	0.10	0.10	0.09	0.13	0.13	0.14	0.11	0.11	0.10
CaO	0.01	0.00	0.00	0.00	0.00	0.00	0.00	0.01	0.00	0.00	0.01
Na2O	0.11	0.11	0.08	0.11	0.15	0.10	0.08	0.09	0.10	0.08	0.07
K2O	2.07	1.99	2.04	2.04	2.03	2.06	2.08	2.03	2.04	2.04	2.04
IV	8.00	8.00	8.00	8.00	8.00	8.00	8.00	8.00	8.00	8.00	8.00
VI	3.97	4.01	4.01	4.02	3.99	3.98	3.99	4.00	4.00	4.01	3.97
Sum Alk.	2.18	2.10	2.12	2.15	2.18	2.16	2.16	2.13	2.14	2.12	2.12
%Mus	0.95	0.95	0.96	0.95	0.93	0.95	0.96	0.95	0.95	0.96	0.96
	94.80	94.83	96.01	94.93	93.29	95.47	96.25	95.25	95.07	96.31	96.25
%par	0.05	0.05	0.04	0.05	0.07	0.05	0.04	0.04	0.05	0.04	0.03
	4.90	5.12	3.96	5.07	6.71	4.53	3.57	4.43	4.83	3.57	3.27
%Mar	0.00	0.00	0.00	0.00	0.00	0.00	0.00	0.00	0.00	0.00	0.00

RM17A Muscovite, Electron microprobe analyses											
Oxide Wt%	**14**	**15**	**16**	**17**	**18**	**20**	**21**	**22**	**23**	**162**	**173**
SiO2	47.01	45.70	45.83	35.00	45.52	46.48	46.04	46.27	46.31	46.42	46.42
TiO2	1.06	0.75	1.13	2.65	1.20	0.83	0.82	0.83	0.75	1.31	0.97
Al2O3	35.21	35.97	34.58	18.45	35.59	35.96	35.28	35.37	35.52	35.35	35.92
FeO	1.69	1.66	3.26	23.89	1.56	1.63	1.69	1.86	1.61	1.81	1.69
MnO	0.05	0.04	0.07	0.51	0.05	0.03	0.07	0.03	0.01	0.05	0.04
MgO	0.70	0.73	1.33	6.68	0.82	0.75	0.80	0.74	0.74	0.86	0.79
CaO	0.00	0.01	0.07	0.02	0.00	0.02	0.02	0.02	0.04	0.00	0.02
Na2O	0.32	0.47	0.40	0.00	0.38	0.47	0.59	0.55	0.42	0.42	0.56
K2O	9.02	10.31	10.16	9.63	11.03	10.84	10.69	10.51	10.72	11.30	10.93
Total	95.06	95.64	96.83	96.84	96.14	97.02	95.99	96.17	96.12	97.52	97.33
Cations (on the basis of 22 O)											
Si	6.21	6.07	6.07	5.38	6.04	6.10	6.11	6.12	6.13	6.09	6.08
Ti	0.11	0.08	0.11	0.31	0.12	0.08	0.08	0.08	0.07	0.13	0.10
AlIV	1.79	1.93	1.93	2.62	1.96	1.90	1.89	1.88	1.87	1.91	1.92
AlVI	3.70	3.70	3.46	0.72	3.61	3.66	3.63	3.64	3.67	3.55	3.63
Fe	0.19	0.18	0.36	3.07	0.17	0.18	0.19	0.21	0.18	0.20	0.18
Mn	0.01	0.00	0.01	0.07	0.01	0.00	0.01	0.00	0.00	0.01	0.00
Mg	0.14	0.14	0.26	1.53	0.16	0.15	0.16	0.15	0.15	0.17	0.15
Ca	0.00	0.00	0.01	0.00	0.00	0.00	0.00	0.00	0.01	0.00	0.00
Na	0.08	0.12	0.10	0.00	0.10	0.12	0.15	0.14	0.11	0.11	0.14
K	1.52	1.75	1.72	1.89	1.87	1.81	1.81	1.77	1.81	1.89	1.83
IV	8.00	8.00	8.00	8.00	8.00	8.00	8.00	8.00	8.00	8.00	8.00
VI	4.14	4.11	4.20	5.70	4.07	4.07	4.06	4.08	4.07	4.05	4.06
Sum Alk.	1.60	1.87	1.83	1.89	1.97	1.94	1.97	1.92	1.92	2.00	1.97
%Mus	0.95	0.93	0.94	1.00	0.95	0.94	0.92	0.93	0.94	0.95	0.93
%Par	0.05	0.07	0.06	0.00	0.05	0.06	0.08	0.07	0.06	0.05	0.07
%Mar	0.00	0.00	0.01	0.00	0.00	0.00	0.00	0.00	0.00	0.00	0.00

T5 Muscovite, Electron microprobe analyses			
Oxide Wt%	**17**	**2**	**11**
SiO2	45.13	46.56	45.66
TiO2	0.7305	0.7899	0.6298
Al2O3	35.48	36.1	36.19
FeO	1.3598	1.6443	1.1547
MnO	0.0355	0.0668	0
MgO	0.7071	0.4683	0.5747
CaO	0.0264	0.0315	0
Na2O	0.7246	0.4183	0.4926
K2O	11.5	9.5	11.47
Total	95.7	95.58	96.18
Cations (on the basis of 22 O)			
SiO2	6.040062	6.14227857	6.0560125
TiO2	0.07354623	0.07838858	0.06283732
AlIV	1.959938	1.85772143	1.9439875
AlVI	3.63714887	3.75568014	3.7137372
FeO	0.15220416	0.18141493	0.12808417
MnO	0.00402453	0.00746456	0
MgO	0.14107378	0.09209374	0.11362698
CaO	0.00378594	0.00445268	0
Na2O	0.18810277	0.10703485	0.1267261
K2O	1.96402683	1.59924005	1.94127824
IV	8	8	8
VI	4.00799758	4.11504194	4.01828566
Sum Alk.	2.15591555	1.71072757	2.06800434
%Mus	0.91099433	0.93483035	0.93872059
	91.0994328	93.4830345	93.8720585
%par	0.0872496	0.06256686	0.06127941
	8.7249599	6.25668568	6.12794147
%Mar	0.00175607	0.0026028	0

RM17A Biotite, Electron microprobe analyses																
Oxide Wt%	**3**	**4**	**5**	**6**	**7**	**8**	**9**	**10**	**11**	**12**	**24**	**25**	**26**	**27**	**28**	**18**
SiO2	34.07	34.66	33.86	35.32	35.52	35.80	35.10	35.06	35.83	35.32	35.04	34.48	35.33	35.20	34.72	34.86
TiO2	2.85	2.88	2.56	3.10	2.74	2.53	2.48	2.51	2.49	2.52	3.05	2.69	3.07	2.77	2.54	3.61
Al2O3	18.56	18.94	17.74	18.94	18.88	18.39	18.34	18.08	18.45	18.04	18.31	17.83	18.52	18.07	18.25	18.79
FeO	22.69	22.68	23.76	21.60	22.41	23.25	23.87	23.96	22.80	23.95	21.98	22.53	21.81	22.50	23.13	23.02
MnO	0.60	0.68	0.53	0.62	0.67	0.64	0.60	0.61	0.58	0.68	0.61	0.59	0.58	0.58	0.54	0.61
MgO	6.08	5.80	5.94	6.07	6.36	5.91	6.12	6.06	5.72	6.00	6.48	5.91	6.37	6.03	6.37	5.91
CaO	0.06	0.06	0.14	0.00	0.06	0.08	0.02	0.02	0.09	0.00	0.03	0.05	0.05	0.00	0.02	0.02
Na2O	0.14	0.04	0.10	0.15	0.06	0.04	0.00	0.07	0.03	0.00	0.17	0.00	0.01	0.00	0.04	0.07
K2O	8.62	8.30	7.72	9.46	9.16	9.11	9.42	9.66	8.52	9.25	8.95	8.77	9.00	8.97	9.04	10.09
Total	93.66	94.04	92.36	95.26	95.85	95.75	95.95	96.02	94.52	95.77	94.63	92.84	94.74	94.12	94.64	96.98
Cations (on the basis of 22 O)																
Si	5.37	5.42	5.43	5.45	5.45	5.52	5.44	5.44	5.56	5.48	5.45	5.48	5.47	5.51	5.43	5.35
Ti	0.34	0.34	0.31	0.36	0.32	0.29	0.29	0.29	0.29	0.29	0.36	0.32	0.36	0.33	0.30	0.42
AlIV	2.63	2.58	2.57	2.55	2.55	2.48	2.56	2.56	2.44	2.52	2.55	2.52	2.53	2.49	2.57	2.65
AlVI	0.82	0.91	0.78	0.89	0.87	0.86	0.79	0.75	0.94	0.78	0.80	0.83	0.85	0.84	0.80	0.74
Fe	2.99	2.97	3.18	2.79	2.88	3.00	3.09	3.11	2.96	3.11	2.86	3.00	2.82	2.95	3.03	2.95
Mn	0.08	0.09	0.07	0.08	0.09	0.08	0.08	0.08	0.08	0.09	0.08	0.08	0.08	0.08	0.07	0.08
Mg	1.43	1.35	1.42	1.40	1.46	1.36	1.41	1.40	1.32	1.39	1.50	1.40	1.47	1.41	1.49	1.35
Ca	0.01	0.01	0.02	0.00	0.01	0.01	0.00	0.00	0.02	0.00	0.01	0.01	0.01	0.00	0.00	0.00
Na	0.04	0.01	0.03	0.04	0.02	0.01	0.00	0.02	0.01	0.00	0.05	0.00	0.00	0.00	0.01	0.02
K	1.73	1.66	1.58	1.86	1.79	1.79	1.86	1.91	1.69	1.83	1.78	1.78	1.78	1.79	1.80	1.97
IV	8.00	8.00	8.00	8.00	8.00	8.00	8.00	8.00	8.00	8.00	8.00	8.00	8.00	8.00	8.00	8.00
VI	5.66	5.65	5.76	5.52	5.61	5.60	5.66	5.64	5.59	5.66	5.60	5.63	5.58	5.60	5.68	5.54
Sum Alk.	1.79	1.68	1.64	1.91	1.82	1.82	1.87	1.94	1.71	1.83	1.83	1.79	1.79	1.79	1.82	2.00
%Ann	0.68	0.69	0.69	0.67	0.66	0.69	0.69	0.69	0.69	0.69	0.66	0.68	0.66	0.68	0.67	0.69
%Phl	0.32	0.31	0.31	0.33	0.34	0.31	0.31	0.31	0.31	0.31	0.34	0.32	0.34	0.32	0.33	0.31

RM15 Biotite, Electron microprobe analyses															
Oxide Wt%	**1**	**2**	**3**	**4**	**12**	**23**	**34**	**45**	**35**	**36**	**37**	**38**	**39**	**40**	**41**
SiO2	34.71	34.69	34.74	34.72	34.71	34.69	34.74	34.72	33.94	36.35	34.62	29.33	35.29	33.09	33.12
TiO2	3.09	3.13	3.03	3.08	3.09	3.13	3.03	3.08	2.00	1.77	2.02	2.45	2.96	2.97	2.92
Al2O3	19.00	18.78	18.66	18.88	19.00	18.78	18.66	18.88	18.51	20.24	18.48	17.95	19.11	18.28	18.45
FeO	22.10	21.82	21.55	21.57	22.10	21.82	21.55	21.57	22.34	20.69	21.27	18.24	20.52	22.08	21.24
MnO	0.63	0.59	0.52	0.60	0.63	0.59	0.52	0.60	0.50	0.47	0.46	0.43	0.55	0.58	0.44
MgO	5.31	5.80	5.20	5.78	5.31	5.80	5.20	5.78	5.87	5.47	5.76	5.71	5.36	6.27	5.94
Na2O	0.00	0.00	0.16	0.07	0.00	0.00	0.16	0.07	0.00	0.00	0.10	0.10	0.07	0.00	0.08
CaO	0.04	0.04	0.01	0.09	0.04	0.04	0.01	0.09	0.05	0.05	0.12	0.06	0.14	0.11	0.22
K2O	10.13	10.09	10.20	10.07	10.13	10.09	10.20	10.07	7.93	7.48	7.72	7.10	9.22	9.39	9.09
Total	95.01	94.93	94.06	94.86	95.01	94.93	94.06	94.86	91.15	92.52	90.52	81.37	93.22	92.77	91.51
Cations (on the basis of 22 O)															
Si	5.41	5.41	5.46	5.41	5.41	5.41	5.46	5.41	5.47	5.64	5.57	5.25	5.53	5.30	5.34
Ti	0.36	0.37	0.36	0.36	0.36	0.37	0.36	0.36	0.24	0.21	0.24	0.33	0.35	0.36	0.35
AlIV	2.59	2.59	2.54	2.59	2.59	2.59	2.54	2.59	2.53	2.36	2.43	2.75	2.47	2.70	2.66
AlVI	0.90	0.86	0.92	0.88	0.90	0.86	0.92	0.88	0.98	1.34	1.07	1.04	1.05	0.75	0.85
Fe	2.88	2.84	2.83	2.81	2.88	2.84	2.83	2.81	3.01	2.68	2.86	2.73	2.69	2.96	2.87
Mn	0.08	0.08	0.07	0.08	0.08	0.08	0.07	0.08	0.07	0.06	0.06	0.07	0.07	0.08	0.06
Mg	1.23	1.35	1.22	1.34	1.23	1.35	1.22	1.34	1.41	1.26	1.38	1.52	1.25	1.50	1.43
Ca	0.00	0.00	0.03	0.01	0.00	0.00	0.03	0.01	0.00	0.00	0.02	0.02	0.01	0.00	0.01
Na	0.01	0.01	0.00	0.03	0.01	0.01	0.00	0.03	0.02	0.02	0.04	0.02	0.04	0.04	0.07
K	2.02	2.01	2.05	2.00	2.02	2.01	2.05	2.00	1.63	1.48	1.58	1.62	1.84	1.92	1.87
IV	8.00	8.00	8.00	8.00	8.00	8.00	8.00	8.00	8.00	8.00	8.00	8.00	8.00	8.00	8.00
VI	5.47	5.49	5.40	5.47	5.47	5.49	5.40	5.47	5.71	5.56	5.61	5.69	5.41	5.64	5.56
Sum Alk.	2.03	2.02	2.08	2.04	2.03	2.02	2.08	2.04	1.65	1.50	1.64	1.66	1.90	1.95	1.96
%ann	0.70	0.68	0.70	0.68	0.70	0.68	0.70	0.68	0.68	0.68	0.67	0.64	0.68	0.66	0.67
%phl	0.30	0.32	0.30	0.32	0.30	0.32	0.30	0.32	0.32	0.32	0.33	0.36	0.32	0.34	0.33

Oxide Wt%	14	15
SiO2	30.52	32.77
TiO2	3.09	3.30
Al2O3	17.48	17.32
FeO	13.52	13.96
MnO	0.19	0.28
MgO	5.51	10.30
CaO	0.00	0.01
Na2O	0.02	0.14
K2O	7.32	8.98
Total	77.67	87.06
Mineral Formulas on the basis of 22 O		
Si	5.55	5.37
Ti	0.42	0.41
AlIV	2.45	2.63
AlVI	1.30	0.71
Fe	2.06	1.91
Mn	0.03	0.04
Mg	1.49	2.52
Ca	0.00	0.00
Na	0.01	0.05
K	1.70	1.88
IV	8.00	8.00
VI	5.30	5.59
Sum Alk.	1.71	1.92
%Ann	0.58	0.43
%Phl	0.42	0.57

APPENDIX C. ARGON DATA

Date Run:	9/15/2017	Elapsed Days:	118
Volts 40Ar from air:	19.741935	Monitors:GA1550 Biotite	9.88E+07
Irradiation Package:	AU-32	FC Sanidine	2.80E+07
Date of Irradiation:	5/17/2017	Air 40Ar/36Ar:	293.5

Fusion analyses were accomplished with a CO2 laser. Data are corrected for interfering nuclear reactions, blank, and mass discrimination. Data are in volts and errors are the standard deviation unless indicated otherwise. Plateau ages include errors arising from precision of measurement and in estimating the J-value. All samples were analyzed within 250 days of irradiation.

Sample RM21 (au32.2q.mus)			28.78±0.31 [1.1%] 95% conf.									
Sample	P	t	40 V	39 V	38 V	37 V	36 V	Moles 40Ar*	%Rad	R	Age (Ma)	%-sd
67	3	10	8.39951 ± 0.003598	1.93426 ± 0.001370	0.0257 ± 0.0002	0.0033 ± 0.00009	0.001592 ± 0.000017	5.00E-14	94.4%	4.0995	28.54 ± 0.03	0.11%
68	3	10	3.33361 ± 0.003057	0.62489 ± 0.000977	0.0087 ± 0.0001	0.0001 ± 0.00004	0.002432 ± 0.000016	1.98E-14	78.4%	4.1848	29.13 ± 0.09	0.29%
69	3	10	7.83194 ± 0.006120	1.51882 ± 0.001028	0.0209 ± 0.0002	0.0004 ± 0.00005	0.005089 ± 0.000044	4.66E-14	80.8%	4.1666	29.01 ± 0.07	0.24%
70	3	10	9.96926 ± 0.003770	1.90622 ± 0.001897	0.0264 ± 0.0001	0.0004 ± 0.00004	0.007483 ± 0.000054	5.93E-14	77.8%	4.0699	28.34 ± 0.07	0.25%
71	3	10	3.75855 ± 0.003333	0.67190 ± 0.000930	0.0091 ± 0.0001	0.0002 ± 0.00004	0.002904 ± 0.000045	2.24E-14	77.2%	4.3169	30.04 ± 0.15	0.50%
72	3	10	9.36100 ± 0.006317	2.16099 ± 0.002720	0.0288 ± 0.0002	0.0010 ± 0.00006	0.001207 ± 0.000030	5.57E-14	96.2%	4.1668	29.01 ± 0.05	0.18%
73	3	10	12.33819 ± 0.008348	2.57612 ± 0.002847	0.0351 ± 0.0004	0.0011 ± 0.00004	0.005914 ± 0.000039	7.34E-14	85.8%	4.1111	28.62 ± 0.05	0.19%
74	3	10	5.64460 ± 0.002232	1.06078 ± 0.001411	0.0146 ± 0.0001	0.0002 ± 0.00005	0.004449 ± 0.000041	3.36E-14	76.7%	4.0818	28.42 ± 0.09	0.33%
75	3	10	4.73822 ± 0.004522	1.09064 ± 0.000579	0.0142 ± 0.0001	0.0001 ± 0.00002	0.000791 ± 0.000014	2.82E-14	95.1%	4.1300	28.75 ± 0.04	0.15%
76	3	10	7.49190 ± 0.004039	1.67749 ± 0.001780	0.0224 ± 0.0002	0.0005 ± 0.00007	0.002120 ± 0.000018	4.46E-14	91.6%	4.0926	28.50 ± 0.04	0.15%
Sample RM20D (au32.2n.mus)			29.80±0.57 [1.9%] 95% conf									
77	3	10	4.76142 ± 0.003142	0.90468 ± 0.001113	0.0120 ± 0.000085	0.00029 ± 0.000058	0.002883 ± 0.000019	2.83E-14	82.1%	4.3216	30.08 ± 0.07	0.22%
78	3	10	6.22002 ± 0.005311	1.44673 ± 0.001784	0.0183 ± 0.000066	0.00875 ± 0.000125	0.000560 ± 0.000011	3.70E-14	97.3%	4.1856	29.14 ± 0.05	0.16%
79	3	10	6.39062 ± 0.006156	1.66388 ± 0.001758	0.0225 ± 0.000125	0.00048 ± 0.000021	0.004374 ± 0.000046	3.80E-14	79.8%	3.0641	21.38 ± 0.07	0.32%
80	3	15	16.02097 ± 0.011403	3.22327 ± 0.002519	0.0430 ± 0.000341	0.00948 ± 0.000107	0.006256 ± 0.000036	9.54E-14	88.5%	4.3971	30.60 ± 0.04	0.14%
81	3	15	16.27433 ± 0.011090	3.79652 ± 0.002261	0.0496 ± 0.000256	0.08106 ± 0.000313	0.001852 ± 0.000020	9.69E-14	96.6%	4.1445	28.85 ± 0.03	0.10%
82	3	15	20.93672 ± 0.008400	4.49032 ± 0.003351	0.0587 ± 0.000182	0.00453 ± 0.000077	0.003476 ± 0.000029	1.25E-13	95.1%	4.4340	30.85 ± 0.03	0.10%
83	3	15	9.30192 ± 0.009424	2.93446 ± 0.003375	0.0377 ± 0.000204	0.00135 ± 0.000058	0.001397 ± 0.000015	5.54E-14	95.6%	3.0293	21.13 ± 0.04	0.17%
84	3	15	13.19549 ± 0.008971	2.96105 ± 0.003175	0.0396 ± 0.000219	0.01032 ± 0.000067	0.001737 ± 0.000021	7.86E-14	96.1%	4.2834	29.81 ± 0.04	0.14%
85	3	15	11.72978 ± 0.007021	2.62566 ± 0.002082	0.0345 ± 0.000272	0.00216 ± 0.000043	0.001596 ± 0.000020	6.98E-14	96.0%	4.2878	29.84 ± 0.03	0.12%
86	3	15	3.64064 ± 0.002170	0.83770 ± 0.001169	0.0108 ± 0.000161	0.00031 ± 0.000033	0.000389 ± 0.000019	2.17E-14	96.8%	4.2088	29.30 ± 0.07	0.23%
Sample RM20D.2 (au32.2o.mus)			28.59±0.43 [1.5%] 95% conf.									
87	3	10	2.13397 ± 0.002420	0.40583 ± 0.000286	0.0053 ± 0.000062	0.00009 ± 0.000040	0.001247 ± 0.000017	1.27E-14	82.7%	4.3504	30.28 ± 0.10	0.33%
88	3	10	7.58192 ± 0.004620	1.17526 ± 0.001174	0.0172 ± 0.000175	0.00035 ± 0.000059	0.009367 ± 0.000072	4.51E-14	63.5%	4.0962	28.52 ± 0.14	0.48%
89	3	10	6.30693 ± 0.005702	1.44397 ± 0.001297	0.0189 ± 0.000098	0.02189 ± 0.000201	0.000785 ± 0.000015	3.75E-14	96.3%	4.2085	29.30 ± 0.04	0.15%
90	3	10	11.08483 ± 0.005196	1.33350 ± 0.002331	0.0207 ± 0.000124	0.00121 ± 0.000033	0.019126 ± 0.000120	6.60E-14	49.0%	4.0745	28.37 ± 0.22	0.77%
91	3	10	9.02190 ± 0.008526	1.84090 ± 0.001602	0.0251 ± 0.000151	0.00023 ± 0.000061	0.004699 ± 0.000029	5.37E-14	84.6%	4.1465	28.87 ± 0.05	0.19%
92	3	10	6.10455 ± 0.004923	1.18781 ± 0.001602	0.0158 ± 0.000079	0.00030 ± 0.000041	0.004585 ± 0.000055	3.63E-14	77.8%	3.9987	27.85 ± 0.11	0.40%
93	3	10	3.40223 ± 0.001506	0.72231 ± 0.001142	0.0096 ± 0.000071	0.00018 ± 0.000039	0.001512 ± 0.000020	2.03E-14	86.9%	4.0918	28.49 ± 0.08	0.28%
94	3	10	10.97747 ± 0.004655	2.56121 ± 0.001735	0.0331 ± 0.000166	0.00089 ± 0.000034	0.001939 ± 0.000027	6.53E-14	94.8%	4.0624	28.29 ± 0.03	0.11%
95	3	10	5.97811 ± 0.005041	1.32602 ± 0.001175	0.0173 ± 0.000078	0.00050 ± 0.000073	0.002021 ± 0.000021	3.56E-14	90.0%	4.0579	28.26 ± 0.05	0.18%
96	3	10	6.86556 ± 0.005644	1.59464 ± 0.001576	0.0207 ± 0.000178	0.00058 ± 0.000044	0.001244 ± 0.000016	4.09E-14	94.6%	4.0749	28.37 ± 0.04	0.15%

Sample RM16A (au32.3b.mus)			21.03±0.20 [0.94%] 95% conf.									
97	3	10	7.06559 ± 0.005122	2.25721 ± 0.001298	0.0297 ± 0.000150	0.00075 ± 0.000054	0.000823 ± 0.000019	4.21E-14	96.6%	3.0226	21.09 ± 0.03	0.13%
98	3	10	8.45968 ± 0.005224	2.76614 ± 0.002295	0.0370 ± 0.000204	0.00378 ± 0.000049	0.000654 ± 0.000023	5.04E-14	97.7%	2.9886	20.85 ± 0.03	0.14%
99	3	10	14.65869 ± 0.012685	4.43292 ± 0.004168	0.0592 ± 0.000256	0.00301 ± 0.000050	0.003554 ± 0.000029	8.73E-14	92.8%	3.0699	21.42 ± 0.03	0.15%
100	3	10	2.23265 ± 0.001441	0.68045 ± 0.001027	0.0090 ± 0.000139	0.00047 ± 0.000046	0.000541 ± 0.000012	1.33E-14	92.8%	3.0462	21.25 ± 0.05	0.24%
101	3	10	6.58114 ± 0.005788	2.08556 ± 0.002585	0.0276 ± 0.000251	0.00166 ± 0.000058	0.000851 ± 0.000014	3.92E-14	96.2%	3.0351	21.18 ± 0.04	0.17%
102	3	10	7.15136 ± 0.001546	2.15916 ± 0.001666	0.0286 ± 0.000128	0.00076 ± 0.000063	0.001972 ± 0.000018	4.26E-14	91.9%	3.0423	21.23 ± 0.02	0.12%
103	3	10	2.89260 ± 0.002568	0.88701 ± 0.001268	0.0121 ± 0.000080	0.00252 ± 0.000078	0.000703 ± 0.000020	1.72E-14	92.8%	3.0271	21.12 ± 0.06	0.28%
104	3	10	2.01095 ± 0.002831	0.57545 ± 0.000928	0.0076 ± 0.000055	0.00322 ± 0.000051	0.001040 ± 0.000012	1.20E-14	84.7%	2.9610	20.66 ± 0.07	0.33%
105	3	10	3.32343 ± 0.002165	0.88829 ± 0.000650	0.0124 ± 0.000067	0.00054 ± 0.000056	0.002297 ± 0.000014	1.98E-14	79.6%	2.9772	20.77 ± 0.04	0.20%
106	3	10	6.87137 ± 0.004862	1.47357 ± 0.001011	0.0214 ± 0.000124	0.00235 ± 0.000058	0.008479 ± 0.000055	4.09E-14	63.5%	2.9629	20.67 ± 0.08	0.41%
Sample RM15 (au32.2a.mus)			21.77±0.34 [1.6%] 95% conf.									
107	3	10	8.94041 ± 0.005490	2.61977 ± 0.002222	0.0353 ± 0.000155	0.00176 ± 0.000071	0.002322 ± 0.000020	5.32E-14	92.3%	3.1508	21.98 ± 0.03	0.13%
108	3	10	3.37331 ± 0.003538	0.96906 ± 0.001075	0.0129 ± 0.000128	0.00107 ± 0.000063	0.001422 ± 0.000015	2.01E-14	87.5%	3.0474	21.26 ± 0.05	0.23%
109	3	10	0.40739 ± 0.001201	0.09052 ± 0.000227	0.0013 ± 0.000023	0.19257 ± 0.000964	0.000303 ± 0.000017	2.43E-15	78.0%	3.7074	25.83 ± 0.40	1.53%
110	3	10	12.89493 ± 0.008972	3.64979 ± 0.004448	0.0473 ± 0.000222	0.01717 ± 0.000157	0.005160 ± 0.000027	7.68E-14	88.2%	3.1157	21.73 ± 0.04	0.17%
113	3	10	9.47969 ± 0.005738	2.38053 ± 0.002339	0.0322 ± 0.000186	0.00157 ± 0.000113	0.007122 ± 0.000051	5.64E-14	77.8%	3.0982	21.61 ± 0.05	0.25%
114	3	10	8.08752 ± 0.002846	2.08492 ± 0.001221	0.0278 ± 0.000155	0.00292 ± 0.000095	0.004987 ± 0.000023	4.81E-14	81.8%	3.1723	22.13 ± 0.03	0.13%
115	3	10	6.46110 ± 0.004825	1.93413 ± 0.001582	0.0254 ± 0.000237	0.02330 ± 0.000213	0.001860 ± 0.000018	3.85E-14	91.5%	3.0567	21.32 ± 0.03	0.15%
116	3	10	6.32002 ± 0.006238	1.79553 ± 0.002909	0.0237 ± 0.000189	0.00080 ± 0.000049	0.002743 ± 0.000017	3.76E-14	87.2%	3.0684	21.41 ± 0.05	0.24%
117	3	10	6.48528 ± 0.002955	1.84676 ± 0.001463	0.0240 ± 0.000186	0.00041 ± 0.000057	0.001562 ± 0.000016	3.86E-14	92.9%	3.2618	22.75 ± 0.03	0.12%
118	3	10	12.03507 ± 0.005852	3.33186 ± 0.002242	0.0442 ± 0.000218	0.02720 ± 0.000189	0.005330 ± 0.000045	7.16E-14	86.9%	3.1397	21.90 ± 0.03	0.16%
Sample RM20D (au32.2n.mus)			20.86±0.46 [2.2%] 95% conf.									
79	3	10	6.39062 ± 0.006156	1.66388 ± 0.001758	0.0225 ± 0.000125	0.00048 ± 0.000021	0.004374 ± 0.000046	3.80E-14	79.8%	3.0641	21.38 ± 0.07	0.32%
79b	0.9	20	0.10141 ± 0.000517	0.02360 ± 0.000126	0.0002 ± 0.000029	0.00005 ± 0.000029	0.000121 ± 0.000012	6.04E-16	64.8%	2.7841	19.43 ± 1.09	5.59%
79c	1	20	0.18077 ± 0.000720	0.04717 ± 0.000346	0.0006 ± 0.000026	0.00005 ± 0.000020	0.000111 ± 0.000016	1.08E-15	81.8%	3.1361	21.88 ± 0.71	3.27%
79d	1.2	20	0.35669 ± 0.000887	0.09074 ± 0.000310	0.0012 ± 0.000027	0.00006 ± 0.000038	0.000297 ± 0.000013	2.12E-15	75.4%	2.9623	20.67 ± 0.31	1.51%
79e	1.4	20	0.48813 ± 0.000691	0.15427 ± 0.000408	0.0020 ± 0.000017	0.00005 ± 0.000027	0.000087 ± 0.000011	2.91E-15	94.7%	2.9977	20.92 ± 0.16	0.78%
79f	1.6	20	0.67634 ± 0.000698	0.21274 ± 0.000702	0.0027 ± 0.000024	0.00004 ± 0.000035	0.000138 ± 0.000012	4.03E-15	94.0%	2.9879	20.85 ± 0.14	0.65%
79g	1.85	20	1.80571 ± 0.001354	0.57712 ± 0.000781	0.0076 ± 0.000123	0.00016 ± 0.000032	0.000207 ± 0.000013	1.07E-14	96.6%	3.0228	21.09 ± 0.06	0.27%
79h	2.1	20	0.49390 ± 0.000525	0.16091 ± 0.000577	0.0019 ± 0.000026	-0.00001 ± 0.000034	0.000014 ± 0.000014	2.94E-15	99.1%	3.0432	21.23 ± 0.20	0.95%
79i	2.4	20	0.05742 ± 0.000584	0.01960 ± 0.000139	0.0002 ± 0.000016	-0.00004 ± 0.000037	-0.000011 ± 0.000015	3.42E-16	105.4%	2.9291	20.44 ± 1.63	7.96%
79j	2.7	20	0.04300 ± 0.000405	0.01393 ± 0.000162	0.0002 ± 0.000011	0.00005 ± 0.000033	0.000011 ± 0.000014	2.56E-16	92.7%	2.8601	19.96 ± 2.14	10.70%
79k	3	20	0.03871 ± 0.000381	0.01266 ± 0.000151	0.0001 ± 0.000011	-0.00004 ± 0.000035	-0.000003 ± 0.000016	2.30E-16	102.0%	3.0568	21.33 ± 2.62	12.26%

Sample RM17A (au32.2d.mus)			21.003±0.084 [0.40%] 95% conf.									
74	2.4	20	2.46792 ± 0.003839	0.76289 ± 0.000679	0.0095 ± 0.000068	0.00143 ± 0.000231	0.000575 ± 0.000018	1.47E-14	93.1%	3.0124	20.99 ± 0.03	0.30%
73	2.5	15	11.46100 ± 0.009702	3.47691 ± 0.003113	0.0456 ± 0.000352	0.01144 ± 0.000292	0.003719 ± 0.000036	6.82E-14	90.4%	2.9803	20.79 ± 0.04	0.17%
75	2.5	15	3.89052 ± 0.003435	1.14241 ± 0.001082	0.0152 ± 0.000140	0.00805 ± 0.000322	0.001576 ± 0.000039	2.32E-14	88.0%	2.9978	20.92 ± 0.08	0.37%
76	2.5	15	6.17453 ± 0.005467	1.92378 ± 0.001698	0.0251 ± 0.000204	0.00152 ± 0.000162	0.001187 ± 0.000020	3.68E-14	94.3%	3.0273	21.12 ± 0.04	0.17%
77	2.5	15	8.55352 ± 0.009633	2.68477 ± 0.002494	0.0348 ± 0.000251	0.00154 ± 0.000288	0.001824 ± 0.000025	5.09E-14	93.7%	2.9852	20.83 ± 0.04	0.18%
78	2.5	15	6.54519 ± 0.005346	1.83918 ± 0.001764	0.0243 ± 0.000159	0.00088 ± 0.000104	0.003274 ± 0.000024	3.90E-14	85.2%	3.0327	21.16 ± 0.04	1.97E-03
79	2.5	15	7.09370 ± 0.006232	1.85076 ± 0.001825	0.0241 ± 0.000167	0.00126 ± 0.000165	0.005042 ± 0.000034	4.22E-14	79.0%	3.0279	21.12 ± 0.05	2.48E-03
80	2.5	15	11.08023 ± 0.007857	3.04044 ± 0.002996	0.0399 ± 0.000212	0.00354 ± 0.000209	0.006554 ± 0.000041	6.60E-14	82.5%	3.0073	20.98 ± 0.04	1.98E-03
81	2.5	15	4.92120 ± 0.005429	1.31714 ± 0.002116	0.0175 ± 0.000107	0.00047 ± 0.000197	0.002997 ± 0.000030	2.93E-14	82.0%	3.0640	21.38 ± 0.07	3.23E-03
82	2.5	15	6.73490 ± 0.009645	1.35634 ± 0.002266	0.0189 ± 0.000115	0.00144 ± 0.000296	0.008986 ± 0.000063	4.01E-14	60.6%	3.0078	20.99 ± 0.12	5.93E-03
83	2.5	15	6.95781 ± 0.002658	1.99822 ± 0.002340	0.0266 ± 0.000164	0.00042 ± 0.000133	0.003122 ± 0.000025	4.14E-14	86.7%	3.0203	21.07 ± 0.04	1.88E-03
84	2.5	15	4.56782 ± 0.003311	1.45311 ± 0.001628	0.0189 ± 0.000174	0.00115 ± 0.000142	0.000750 ± 0.000023	2.72E-14	95.1%	2.9909	20.87 ± 0.04	2.11E-03
85	2.5	15	4.11379 ± 0.003396	1.04034 ± 0.001244	0.0140 ± 0.000142	0.00066 ± 0.000250	0.003275 ± 0.000028	2.45E-14	76.5%	3.0242	21.10 ± 0.07	3.26E-03
86	2.5	15	4.26153 ± 0.001824	1.20614 ± 0.001336	0.0163 ± 0.000173	-0.00023 ± 0.000252	0.002236 ± 0.000042	2.54E-14	84.5%	2.9854	20.83 ± 0.08	3.74E-03
87	2.5	15	3.21577 ± 0.002434	0.89843 ± 0.001045	0.0118 ± 0.000138	0.00046 ± 0.000179	0.001737 ± 0.000025	1.91E-14	84.0%	3.0081	20.99 ± 0.07	3.17E-03
Sample RM19A (au32.2m.mus)			28.10±0.23 [0.81%] 95% conf.									
88	2.5	15	7.77623 ± 0.002202	1.50067 ± 0.001931	0.0208 ± 0.000143	0.00055 ± 0.000188	0.005994 ± 0.000062	4.63E-14	77.2%	4.0015	27.87 ± 0.10	3.53E-03
89	2.5	15	9.78352 ± 0.009857	1.84809 ± 0.001341	0.0256 ± 0.000150	0.00091 ± 0.000184	0.007742 ± 0.000057	5.82E-14	76.6%	4.0560	28.24 ± 0.08	2.77E-03
90	2.5	15	5.04138 ± 0.003214	1.11781 ± 0.002592	0.0149 ± 0.000100	0.00109 ± 0.000215	0.001950 ± 0.000022	3.00E-14	88.6%	3.9945	27.82 ± 0.09	3.08E-03
94	2.5	15	5.16660 ± 0.004764	0.93462 ± 0.001268	0.0126 ± 0.000061	-0.00137 ± 0.000209	0.004624 ± 0.000031	3.08E-14	73.6%	4.0662	28.31 ± 0.09	3.33E-03
95	2.5	15	2.77600 ± 0.001482	0.57125 ± 0.000797	0.0075 ± 0.000063	-0.00057 ± 0.000211	0.001440 ± 0.000028	1.65E-14	84.7%	4.1148	28.65 ± 0.11	3.99E-03
96	2.5	15	6.37378 ± 0.003403	1.40282 ± 0.000743	0.0189 ± 0.000142	-0.00077 ± 0.000106	0.002089 ± 0.000028	3.79E-14	90.3%	4.1035	28.57 ± 0.05	1.68E-03
97	2.5	15	7.61166 ± 0.013352	1.84134 ± 0.002612	0.0238 ± 0.000083	-0.00051 ± 0.000374	0.001105 ± 0.000033	4.53E-14	95.7%	3.9565	27.55 ± 0.07	2.72E-03
98	2.5	15	7.19688 ± 0.004808	1.56995 ± 0.001107	0.0212 ± 0.000121	-0.00087 ± 0.000091	0.003118 ± 0.000029	4.28E-14	87.2%	3.9973	27.84 ± 0.05	1.76E-03
99	2.5	15	3.00925 ± 0.003177	0.70383 ± 0.000773	0.0090 ± 0.000088	-0.00007 ± 0.000192	0.000489 ± 0.000029	1.79E-14	95.2%	4.0701	28.34 ± 0.10	3.43E-03
100	2.5	15	7.46396 ± 0.007669	1.23441 ± 0.001041	0.0177 ± 0.000133	0.00039 ± 0.000239	0.008494 ± 0.000067	4.44E-14	66.4%	4.0132	27.95 ± 0.13	4.48E-03
101	2.5	15	1.94279 ± 0.001858	0.40922 ± 0.000777	0.0053 ± 0.000044	-0.00052 ± 0.000227	0.001042 ± 0.000037	1.16E-14	84.2%	3.9953	27.82 ± 0.20	7.22E-03
102	2.5	15	2.38149 ± 0.002603	0.53433 ± 0.000416	0.0071 ± 0.000083	-0.00018 ± 0.000233	0.000705 ± 0.000036	1.42E-14	91.2%	4.0669	28.32 ± 0.14	5.09E-03
Sample T5 (au32.8n.mus)			25.11±0.48 [1.9%] 95% conf.									
103	2.5	15	2.29420 ± 0.001303	0.43385 ± 0.000797	0.0058 ± 0.000058	-0.00008 ± 0.000170	0.001336 ± 0.000029	1.37E-14	82.8%	4.3778	30.46 ± 0.16	5.10E-03
104	2.5	15	0.98761 ± 0.000845	0.24150 ± 0.000725	0.0032 ± 0.000049	0.00029 ± 0.000170	0.000486 ± 0.000018	5.88E-15	85.5%	3.4946	24.36 ± 0.18	7.32E-03
105	2.5	15	2.02260 ± 0.002099	0.54525 ± 0.000931	0.0071 ± 0.000082	0.00010 ± 0.000296	0.000340 ± 0.000017	1.20E-14	95.0%	3.5252	24.57 ± 0.08	3.34E-03
106	2.5	15	1.73454 ± 0.001561	0.45650 ± 0.000718	0.0059 ± 0.000055	0.00046 ± 0.000172	0.000405 ± 0.000017	1.03E-14	93.1%	3.5372	24.65 ± 0.09	3.67E-03
107	2.5	15	1.52039 ± 0.001754	0.40019 ± 0.000391	0.0051 ± 0.000065	-0.00012 ± 0.000193	0.000256 ± 0.000018	9.05E-15	95.0%	3.6102	25.16 ± 0.10	4.01E-03
108	2.5	15	0.36754 ± 0.000806	0.09590 ± 0.000345	0.0012 ± 0.000024	0.00066 ± 0.000166	0.000114 ± 0.000026	2.19E-15	90.9%	3.4821	24.27 ± 0.56	2.32E-02
109	2.5	15	1.64579 ± 0.001226	0.42213 ± 0.000613	0.0054 ± 0.000046	0.00043 ± 0.000179	0.000284 ± 0.000018	9.80E-15	94.9%	3.6999	25.78 ± 0.10	3.89E-03
110	2.5	15	1.78088 ± 0.001168	0.46033 ± 0.000791	0.0058 ± 0.000049	0.00006 ± 0.000140	0.000510 ± 0.000018	1.06E-14	91.5%	3.5417	24.69 ± 0.09	3.82E-03
113	2.5	15	2.18132 ± 0.001455	0.58847 ± 0.000688	0.0076 ± 0.000079	0.00072 ± 0.000170	0.000444 ± 0.000014	1.30E-14	94.0%	3.4839	24.29 ± 0.06	2.43E-03
114	2.5	15	1.07925 ± 0.001305	0.25731 ± 0.000575	0.0034 ± 0.000038	0.00053 ± 0.000160	0.000369 ± 0.000016	6.42E-15	89.9%	3.7704	26.27 ± 0.15	5.73E-03
115	2.5	15	1.04918 ± 0.001465	0.27366 ± 0.000441	0.0034 ± 0.000030	0.00043 ± 0.000243	0.000039 ± 0.000027	6.25E-15	98.9%	3.7921	26.42 ± 0.21	7.90E-03
116	2.5	15	1.11399 ± 0.001110	0.29607 ± 0.000738	0.0038 ± 0.000036	0.00051 ± 0.000209	0.000213 ± 0.000016	6.63E-15	94.4%	3.5502	24.74 ± 0.13	5.31E-03
117	2.5	15	1.98137 ± 0.001869	0.48714 ± 0.000702	0.0062 ± 0.000043	0.00020 ± 0.000183	0.000628 ± 0.000020	1.18E-14	90.6%	3.6862	25.69 ± 0.10	3.79E-03
118	2.5	15	0.56024 ± 0.000538	0.12711 ± 0.000495	0.0016 ± 0.000030	0.00002 ± 0.000162	0.000309 ± 0.000018	3.34E-15	83.7%	3.6899	25.71 ± 0.32	1.23E-02

Sample RM4 (au32.1c.bio)			33.5±2.0 [6.0%] 95% conf.									
3	2.2	15	2.03159 ± 0.002329	0.26795 ± 0.000512	0.0084 ± 0.000065	0.10636 ± 0.000966	0.002410 ± 0.000021	1.21E-14	65.0%	4.9618	34.49 ± 0.20	5.80E-03
4	2.2	15	11.88055 ± 0.006165	2.00680 ± 0.001873	0.0487 ± 0.000155	0.39301 ± 0.000739	0.007389 ± 0.000044	7.07E-14	81.6%	4.8505	33.72 ± 0.06	1.88E-03
5	2.6	15	7.94473 ± 0.004705	1.36334 ± 0.001417	0.0493 ± 0.000226	0.16167 ± 0.001344	0.003091 ± 0.000023	4.73E-14	88.5%	5.1686	35.91 ± 0.06	1.66E-03
6	2.6	15	9.08957 ± 0.005807	1.30739 ± 0.001511	0.0371 ± 0.000239	0.20915 ± 0.001658	0.011664 ± 0.000074	5.41E-14	62.1%	4.3311	30.14 ± 0.13	4.45E-03
7	2.6	15	5.18272 ± 0.004334	0.55130 ± 0.001212	0.0237 ± 0.000173	0.20489 ± 0.001340	0.010900 ± 0.000044	3.09E-14	37.9%	3.5930	25.04 ± 0.24	9.69E-03
8	2.6	15	2.30767 ± 0.002533	0.41849 ± 0.000752	0.0067 ± 0.000061	0.01258 ± 0.000335	0.000527 ± 0.000017	1.37E-14	93.3%	5.1451	35.75 ± 0.11	3.21E-03
11	2.6	40	1.01161 ± 0.001496	0.10557 ± 0.000320	0.0046 ± 0.000031	0.00706 ± 0.000266	0.002253 ± 0.000048	6.02E-15	34.2%	3.2815	22.88 ± 0.96	4.21E-02
12	2.6	40	2.22752 ± 0.001322	0.36821 ± 0.000432	0.0133 ± 0.000075	0.03804 ± 0.000876	0.001045 ± 0.000024	1.33E-14	86.1%	5.2206	36.27 ± 0.14	3.96E-03
13	2.6	15	9.69679 ± 0.006087	1.33445 ± 0.001401	0.0492 ± 0.000256	0.73825 ± 0.002930	0.010836 ± 0.000088	5.77E-14	67.0%	4.9188	34.19 ± 0.15	4.37E-03
14	2.6	15	5.30142 ± 0.003879	0.88864 ± 0.001764	0.0294 ± 0.000140	0.33799 ± 0.003028	0.002677 ± 0.000041	3.16E-14	85.1%	5.1113	35.52 ± 0.13	3.66E-03
15	2.6	15	4.74300 ± 0.002330	0.79379 ± 0.000990	0.0178 ± 0.000182	0.18855 ± 0.001165	0.002939 ± 0.000024	2.82E-14	81.7%	4.9034	34.09 ± 0.08	2.44E-03
16	2.6	15	2.75773 ± 0.002041	0.36782 ± 0.000353	0.0141 ± 0.000146	0.07646 ± 0.000691	0.003890 ± 0.000055	1.64E-14	58.3%	4.3914	30.56 ± 0.32	1.04E-02
17	2.6	15	10.87503 ± 0.004916	1.80538 ± 0.002164	0.0681 ± 0.000616	0.19960 ± 0.001004	0.005537 ± 0.000042	6.47E-14	85.0%	5.1277	35.63 ± 0.07	2.03E-03
18	2.6	15	7.43637 ± 0.005971	1.27536 ± 0.001428	0.0405 ± 0.000156	0.19254 ± 0.001604	0.003266 ± 0.000028	4.43E-14	87.0%	5.0882	35.36 ± 0.07	2.03E-03
19	2.6	15	3.34805 ± 0.003783	0.55272 ± 0.000583	0.0200 ± 0.000154	0.05147 ± 0.000799	0.001833 ± 0.000030	1.99E-14	83.8%	5.0862	35.35 ± 0.13	3.63E-03
Sample RM6 (au32.1h.bio)			35.62±0.15 [0.41%] 95% conf.									
20	2.6	15	13.14336 ± 0.006487	2.48645 ± 0.001983	0.0407 ± 0.000330	0.09312 ± 0.000707	0.001524 ± 0.000034	7.82E-14	96.6%	5.1083	35.50 ± 0.04	1.26E-03
21	2.6	15	3.29607 ± 0.002576	0.59278 ± 0.000699	0.0097 ± 0.000087	0.01734 ± 0.000279	0.000869 ± 0.000019	1.96E-14	92.2%	5.1301	35.65 ± 0.09	2.41E-03
22	2.6	15	18.26872 ± 0.010764	3.39363 ± 0.002603	0.0566 ± 0.000366	0.21244 ± 0.000746	0.003010 ± 0.000030	1.09E-13	95.1%	5.1270	35.63 ± 0.04	1.14E-03
23	2.6	15	9.60919 ± 0.010363	1.78314 ± 0.001127	0.0290 ± 0.000177	0.07081 ± 0.000611	0.001331 ± 0.000021	5.72E-14	95.9%	5.1720	35.94 ± 0.05	1.47E-03
24	2.6	15	3.24918 ± 0.002007	0.57290 ± 0.000843	0.0094 ± 0.000060	0.02063 ± 0.000303	0.001149 ± 0.000019	1.93E-14	89.5%	5.0821	35.32 ± 0.09	2.64E-03
25	2.6	15	3.05937 ± 0.002972	0.52642 ± 0.000701	0.0087 ± 0.000092	0.09328 ± 0.001378	0.001354 ± 0.000021	1.82E-14	86.9%	5.0680	35.22 ± 0.11	2.99E-03
26	2.6	15	5.69757 ± 0.003135	1.04610 ± 0.001449	0.0178 ± 0.000177	0.06081 ± 0.000899	0.000981 ± 0.000035	3.39E-14	94.9%	5.1748	35.96 ± 0.09	2.49E-03
27	2.6	15	9.42104 ± 0.007852	1.72270 ± 0.001739	0.0291 ± 0.000246	0.07118 ± 0.000881	0.001934 ± 0.000023	5.61E-14	93.9%	5.1409	35.72 ± 0.06	1.60E-03
28	2.6	15	1.24264 ± 0.001802	0.21389 ± 0.000648	0.0035 ± 0.000052	0.02067 ± 0.000292	0.000475 ± 0.000019	7.40E-15	88.7%	5.1630	35.87 ± 0.23	6.35E-03
29	2.6	15	8.56627 ± 0.006131	1.59008 ± 0.001943	0.0261 ± 0.000147	0.07895 ± 0.000681	0.001510 ± 0.000023	5.10E-14	94.8%	5.1113	35.52 ± 0.06	1.70E-03
30	2.6	15	5.68618 ± 0.004627	0.99020 ± 0.001073	0.0170 ± 0.000147	0.03963 ± 0.000538	0.002116 ± 0.000040	3.38E-14	89.0%	5.1148	35.54 ± 0.10	2.80E-03
31	2.6	15	3.97388 ± 0.003156	0.73096 ± 0.001404	0.0115 ± 0.000073	0.02837 ± 0.000554	0.000987 ± 0.000024	2.37E-14	92.7%	5.0411	35.04 ± 0.10	2.94E-03
32	2.6	15	8.62981 ± 0.005752	1.66506 ± 0.001818	0.0274 ± 0.000191	0.09126 ± 0.000772	0.000276 ± 0.000036	5.14E-14	99.1%	5.1391	35.71 ± 0.06	1.80E-03
33	2.6	15	16.36549 ± 0.008748	3.09140 ± 0.002040	0.0518 ± 0.000288	0.23948 ± 0.001550	0.001690 ± 0.000027	9.74E-14	96.9%	5.1396	35.71 ± 0.04	1.01E-03
34	2.6	15	7.97784 ± 0.008825	1.43516 ± 0.002998	0.0235 ± 0.000131	0.05428 ± 0.000577	0.001958 ± 0.000025	4.75E-14	92.7%	5.1592	35.85 ± 0.10	2.74E-03
Sample RM8A (au32.1k.mus)			21.70±0.22 [1.0%] 95% conf.									
35	2.6	15	5.99354 ± 0.004335	1.67776 ± 0.001435	0.0225 ± 0.000204	0.00201 ± 0.000281	0.002799 ± 0.000030	3.57E-14	86.2%	3.0794	21.48 ± 0.05	2.16E-03
36	2.6	15	3.95961 ± 0.003275	0.84024 ± 0.000957	0.0118 ± 0.000102	0.00035 ± 0.000224	0.004696 ± 0.000056	2.36E-14	65.0%	3.0611	21.36 ± 0.15	6.80E-03
37	2.6	15	3.70060 ± 0.001263	1.05337 ± 0.000803	0.0140 ± 0.000081	0.00079 ± 0.000209	0.001473 ± 0.000026	2.20E-14	88.2%	3.0998	21.62 ± 0.06	2.56E-03
38	2.6	15	2.19419 ± 0.002119	0.64257 ± 0.000375	0.0082 ± 0.000041	-0.00005 ± 0.000204	0.000734 ± 0.000026	1.31E-14	90.1%	3.0770	21.47 ± 0.09	4.06E-03
39	2.6	15	5.21679 ± 0.003633	1.33750 ± 0.001244	0.0178 ± 0.000168	0.00097 ± 0.000389	0.003605 ± 0.000050	3.11E-14	79.6%	3.1040	21.65 ± 0.08	3.86E-03
40	2.6	15	3.91566 ± 0.002858	1.11714 ± 0.001563	0.0148 ± 0.000158	0.00080 ± 0.000257	0.001456 ± 0.000029	2.33E-14	89.0%	3.1201	21.76 ± 0.07	3.02E-03
41	2.6	15	12.23540 ± 0.006827	3.52205 ± 0.003306	0.0468 ± 0.000312	0.00310 ± 0.000347	0.004380 ± 0.000035	7.28E-14	89.4%	3.1066	21.67 ± 0.03	1.55E-03
42	2.6	15	15.74967 ± 0.006081	4.36453 ± 0.004348	0.0573 ± 0.000251	0.00613 ± 0.000335	0.007753 ± 0.000046	9.38E-14	85.5%	3.0838	21.51 ± 0.03	1.61E-03

43	2.6	15	2.78286 ± 0.002914	0.80021 ± 0.001226	0.0103 ± 0.000069	0.00169 ± 0.000305	0.001079 ± 0.000019	1.66E-14	88.5%	3.0793	21.48 ± 0.07	3.06E-03
44	2.6	15	7.21468 ± 0.004915	1.90502 ± 0.001747	0.0255 ± 0.000177	0.00201 ± 0.000350	0.003910 ± 0.000029	4.29E-14	84.0%	3.1808	22.19 ± 0.04	1.96E-03
45	2.6	15	4.05207 ± 0.002767	1.01248 ± 0.001658	0.0138 ± 0.000183	0.00120 ± 0.000215	0.002892 ± 0.000025	2.41E-14	78.9%	3.1582	22.03 ± 0.07	3.26E-03
46	2.6	15	2.91138 ± 0.001355	0.74667 ± 0.000895	0.0099 ± 0.000064	0.00134 ± 0.000290	0.001586 ± 0.000028	1.73E-14	83.9%	3.2716	22.81 ± 0.09	3.76E-03
47	2.6	15	6.81423 ± 0.004341	2.00686 ± 0.001353	0.0262 ± 0.000100	0.00107 ± 0.000258	0.002198 ± 0.000022	4.06E-14	90.5%	3.0719	21.43 ± 0.03	1.48E-03
48	2.6	15	9.91852 ± 0.010087	2.99497 ± 0.001570	0.0392 ± 0.000206	0.00147 ± 0.000324	0.001145 ± 0.000034	5.90E-14	96.6%	3.1988	22.31 ± 0.04	1.58E-03
49	2.6	15	8.17302 ± 0.006587	2.28718 ± 0.001625	0.0309 ± 0.000227	0.00203 ± 0.000258	0.004038 ± 0.000028	4.87E-14	85.4%	3.0518	21.29 ± 0.04	1.72E-03
Sample RM9C (au32.1o.mus)			21.74±0.14 [0.62%] 95% conf.									
50	2.6	15	7.03110 ± 0.006889	2.20376 ± 0.001718	0.0278 ± 0.000122	0.00245 ± 0.000272	0.000747 ± 0.000020	4.19E-14	96.9%	3.0905	21.56 ± 0.03	1.55E-03
51	2.6	15	10.54657 ± 0.004284	3.18541 ± 0.003329	0.0410 ± 0.000185	0.00155 ± 0.000222	0.002452 ± 0.000033	6.28E-14	93.1%	3.0834	21.51 ± 0.03	1.56E-03
52	2.6	15	3.99923 ± 0.003059	1.25056 ± 0.001094	0.0158 ± 0.000103	-0.00129 ± 0.000271	0.000246 ± 0.000016	2.38E-14	98.2%	3.1397	21.90 ± 0.04	1.71E-03
53	2.6	15	0.98216 ± 0.001295	0.28719 ± 0.000666	0.0037 ± 0.000057	-0.00179 ± 0.000368	0.000250 ± 0.000019	5.85E-15	92.5%	3.1620	22.06 ± 0.15	6.72E-03
54	2.6	15	13.78198 ± 0.007210	4.19592 ± 0.003555	0.0539 ± 0.000114	0.00687 ± 0.000237	0.002367 ± 0.000029	8.20E-14	94.9%	3.1181	21.75 ± 0.03	1.23E-03
55	2.6	15	3.46614 ± 0.001170	0.97710 ± 0.000560	0.0130 ± 0.000153	-0.00139 ± 0.000300	0.001413 ± 0.000020	2.06E-14	88.0%	3.1200	21.76 ± 0.05	2.09E-03
56	2.6	15	3.20504 ± 0.002883	0.92284 ± 0.001174	0.0123 ± 0.000084	-0.00004 ± 0.000340	0.001042 ± 0.000016	1.91E-14	90.4%	3.1394	21.90 ± 0.05	2.38E-03
57	2.6	15	5.35737 ± 0.004929	1.62361 ± 0.001883	0.0208 ± 0.000078	-0.00170 ± 0.000337	0.001097 ± 0.000018	3.19E-14	93.9%	3.0999	21.62 ± 0.04	1.90E-03
58	2.6	15	3.72704 ± 0.003477	1.14075 ± 0.001284	0.0145 ± 0.000103	-0.00142 ± 0.000163	0.000670 ± 0.000017	2.22E-14	94.7%	3.0936	21.58 ± 0.05	2.12E-03
59	2.6	15	5.02712 ± 0.003939	1.41062 ± 0.000770	0.0188 ± 0.000089	-0.00142 ± 0.000254	0.001908 ± 0.000020	2.99E-14	88.8%	3.1640	22.07 ± 0.04	1.72E-03
60	2.6	15	14.03742 ± 0.008835	4.28963 ± 0.003902	0.0571 ± 0.000249	0.00287 ± 0.000293	0.002797 ± 0.000029	8.36E-14	94.1%	3.0798	21.49 ± 0.03	1.35E-03
61	2.6	15	2.49137 ± 0.001004	0.66669 ± 0.000438	0.0090 ± 0.000091	0.00067 ± 0.000383	0.001415 ± 0.000022	1.48E-14	83.2%	3.1100	21.69 ± 0.07	3.21E-03
62	2.6	15	2.96798 ± 0.002421	0.86622 ± 0.001206	0.0110 ± 0.000059	0.00144 ± 0.000248	0.000838 ± 0.000024	1.77E-14	91.7%	3.1405	21.91 ± 0.07	3.14E-03
63	2.6	15	5.76312 ± 0.004349	1.35625 ± 0.001512	0.0181 ± 0.000117	0.00028 ± 0.000280	0.005007 ± 0.000034	3.43E-14	74.3%	3.1584	22.03 ± 0.07	3.00E-03
64	2.6	15	13.20651 ± 0.005203	4.17229 ± 0.001774	0.0554 ± 0.000454	0.00602 ± 0.000316	0.001647 ± 0.000028	7.86E-14	96.3%	3.0488	21.27 ± 0.02	8.88E-04
Sample RM12 (au32.1q.bio)			26.06±0.27 [1.0%] 95% conf.									
65	2.6	15	1.90566 ± 0.001824	0.48866 ± 0.001622	0.0118 ± 0.000072	0.00254 ± 0.000310	0.000275 ± 0.000016	1.13E-14	95.7%	3.7338	26.02 ± 0.12	4.47E-03
66	2.6	15	1.92394 ± 0.001497	0.49608 ± 0.000969	0.0128 ± 0.000100	0.00088 ± 0.000358	0.000370 ± 0.000017	1.15E-14	94.3%	3.6578	25.49 ± 0.09	3.58E-03
67	2.6	15	7.23480 ± 0.005687	1.78908 ± 0.001975	0.0441 ± 0.000145	0.00255 ± 0.000447	0.002025 ± 0.000019	4.31E-14	91.7%	3.7096	25.85 ± 0.04	1.70E-03
68	2.6	15	4.01433 ± 0.004301	0.97105 ± 0.001568	0.0259 ± 0.000120	0.00216 ± 0.000304	0.001163 ± 0.000021	2.39E-14	91.4%	3.7802	26.34 ± 0.07	2.73E-03
69	2.6	15	3.38626 ± 0.002243	0.78805 ± 0.000916	0.0202 ± 0.000179	0.00342 ± 0.000204	0.001253 ± 0.000020	2.02E-14	89.1%	3.8274	26.66 ± 0.07	2.49E-03
70	2.6	15	0.22723 ± 0.000519	0.00466 ± 0.000162	0.0000 ± 0.000030	0.00138 ± 0.000277	0.000039 ± 0.000017	1.35E-15	94.9%	46.3453	299.03 ± 13.01	4.35E-02
71	2.6	15	5.08211 ± 0.003470	1.29244 ± 0.001372	0.0314 ± 0.000235	0.00508 ± 0.000371	0.001241 ± 0.000021	3.03E-14	92.8%	3.6487	25.43 ± 0.05	1.89E-03
72	2.6	15	5.28172 ± 0.001935	1.33489 ± 0.001580	0.0308 ± 0.000264	0.00677 ± 0.000272	0.000977 ± 0.000018	3.14E-14	94.5%	3.7408	26.06 ± 0.04	1.70E-03
73	2.6	15	6.77431 ± 0.005381	1.65701 ± 0.001836	0.0470 ± 0.000194	0.00418 ± 0.000313	0.002035 ± 0.000022	4.03E-14	91.1%	3.7256	25.96 ± 0.05	1.83E-03
74	2.6	15	0.99622 ± 0.001202	0.24998 ± 0.000488	0.0065 ± 0.000087	0.00118 ± 0.000331	0.000265 ± 0.000018	5.93E-15	92.1%	3.6723	25.59 ± 0.16	6.23E-03
75	2.6	15	0.94535 ± 0.001316	0.23917 ± 0.000339	0.0057 ± 0.000063	0.00205 ± 0.000263	0.000148 ± 0.000019	5.63E-15	95.4%	3.7702	26.27 ± 0.17	6.49E-03
76	2.6	15	0.45696 ± 0.000358	0.10724 ± 0.000359	0.0024 ± 0.000040	0.00068 ± 0.000264	0.000158 ± 0.000015	2.72E-15	89.8%	3.8271	26.66 ± 0.31	1.15E-02
77	2.6	15	0.76690 ± 0.000684	0.17686 ± 0.000483	0.0044 ± 0.000066	0.00116 ± 0.000278	0.000170 ± 0.000014	4.57E-15	93.5%	4.0533	28.22 ± 0.19	6.57E-03
78	2.6	15	7.19827 ± 0.003107	1.87360 ± 0.000852	0.0438 ± 0.000210	0.00098 ± 0.000196	0.000454 ± 0.000018	4.28E-14	98.1%	3.7704	26.27 ± 0.03	9.86E-04
79	2.6	15	2.19711 ± 0.002051	0.57110 ± 0.000397	0.0137 ± 0.000072	0.00018 ± 0.000292	0.000264 ± 0.000015	1.31E-14	96.5%	3.7107	25.86 ± 0.06	2.47E-03

Sample 20C (au32.2i.mus)			29.79±0.26 [0.89%] 95% conf.									
80	2.6	15	9.76545 ± 0.004868	2.16460 ± 0.002060	0.0281 ± 0.000180	0.00132 ± 0.000344	0.001809 ± 0.000022	5.81E-14	94.5%	4.2645	29.68 ± 0.04	1.35E-03
81	2.6	15	3.37215 ± 0.002306	0.79243 ± 0.001228	0.0102 ± 0.000092	0.00118 ± 0.000299	0.000072 ± 0.000015	2.01E-14	99.4%	4.2288	29.44 ± 0.06	2.17E-03
82	2.6	15	12.59751 ± 0.012732	2.80756 ± 0.002970	0.0363 ± 0.000149	0.00469 ± 0.000244	0.002214 ± 0.000032	7.50E-14	94.8%	4.2541	29.61 ± 0.05	1.73E-03
83	2.6	15	4.16418 ± 0.002765	0.95103 ± 0.001327	0.0119 ± 0.000073	0.00179 ± 0.000245	0.000489 ± 0.000017	2.48E-14	96.5%	4.2270	29.42 ± 0.06	2.02E-03
84	2.6	15	10.65414 ± 0.004873	2.36760 ± 0.001685	0.0310 ± 0.000251	0.00815 ± 0.000269	0.001717 ± 0.000032	6.34E-14	95.2%	4.2860	29.83 ± 0.04	1.30E-03
85	2.6	15	9.08882 ± 0.006238	1.99459 ± 0.001529	0.0258 ± 0.000065	0.00094 ± 0.000376	0.001159 ± 0.000019	5.41E-14	96.2%	4.3851	30.51 ± 0.04	1.24E-03
86	2.6	15	7.65254 ± 0.003784	1.74776 ± 0.001689	0.0222 ± 0.000136	0.00717 ± 0.000224	0.000686 ± 0.000029	4.56E-14	97.4%	4.2629	29.67 ± 0.05	1.60E-03
87	2.6	15	7.05398 ± 0.004167	1.55913 ± 0.001119	0.0198 ± 0.000105	0.00444 ± 0.000288	0.001317 ± 0.000019	4.20E-14	94.5%	4.2750	29.75 ± 0.04	1.28E-03
88	2.6	15	12.31883 ± 0.008342	2.89771 ± 0.002134	0.0370 ± 0.000153	0.00776 ± 0.000359	0.001525 ± 0.000045	7.33E-14	96.3%	4.0959	28.52 ± 0.04	1.53E-03
89	2.6	15	6.39878 ± 0.005775	1.29197 ± 0.002139	0.0173 ± 0.000145	0.00373 ± 0.000337	0.003071 ± 0.000024	3.81E-14	85.8%	4.2506	29.59 ± 0.08	2.55E-03
90	2.6	15	3.51592 ± 0.003119	0.77394 ± 0.001298	0.0102 ± 0.000090	0.00131 ± 0.000375	0.000486 ± 0.000015	2.09E-14	95.9%	4.3574	30.32 ± 0.07	2.39E-03
91	2.6	15	6.45830 ± 0.003205	1.37695 ± 0.001046	0.0177 ± 0.000071	0.00108 ± 0.000182	0.001286 ± 0.000029	3.84E-14	94.1%	4.4144	30.72 ± 0.05	1.70E-03
92	2.6	15	3.25166 ± 0.002329	0.68694 ± 0.000960	0.0092 ± 0.000121	0.00344 ± 0.000283	0.001059 ± 0.000030	1.94E-14	90.4%	4.2784	29.78 ± 0.10	3.45E-03
93	2.6	15	3.54485 ± 0.002634	0.73915 ± 0.000941	0.0096 ± 0.000072	0.00032 ± 0.000298	0.001193 ± 0.000032	2.11E-14	90.1%	4.3191	30.06 ± 0.10	3.40E-03
94	2.6	15	1.16138 ± 0.001038	0.25558 ± 0.000450	0.0032 ± 0.000021	-0.00004 ± 0.000416	0.000238 ± 0.000028	6.91E-15	94.0%	4.2692	29.71 ± 0.23	7.90E-03
RM22 (au32.9s.mus)			28.61±0.44 [1.5%] 95% conf.									
95	2.6	15	2.29045 ± 0.002816	0.50817 ± 0.000925	0.0067 ± 0.000071	0.00072 ± 0.000341	0.000911 ± 0.000028	1.36E-14	88.3%	3.9778	27.70 ± 0.13	4.75E-03
96	2.6	15	0.97710 ± 0.001488	0.23433 ± 0.000627	0.0033 ± 0.000044	0.00185 ± 0.000385	0.000148 ± 0.000025	5.82E-15	95.5%	3.9833	27.74 ± 0.24	8.67E-03
97	2.6	15	2.18501 ± 0.001528	0.51540 ± 0.001084	0.0066 ± 0.000071	0.00091 ± 0.000347	0.000318 ± 0.000023	1.30E-14	95.7%	4.0574	28.25 ± 0.11	4.03E-03
98	2.6	15	1.53329 ± 0.001302	0.36805 ± 0.000807	0.0047 ± 0.000054	0.00192 ± 0.000242	0.000222 ± 0.000024	9.13E-15	95.7%	3.9880	27.77 ± 0.15	5.45E-03
99	2.6	15	2.72511 ± 0.002980	0.64195 ± 0.000521	0.0084 ± 0.000047	0.00163 ± 0.000303	0.000750 ± 0.000026	1.62E-14	91.9%	3.9000	27.16 ± 0.09	3.38E-03
100	2.6	15	2.55045 ± 0.001586	0.59085 ± 0.000437	0.0080 ± 0.000083	0.00167 ± 0.000208	0.000679 ± 0.000039	1.52E-14	92.1%	3.9772	27.70 ± 0.14	4.99E-03
101	2.6	15	4.41406 ± 0.002365	0.97939 ± 0.001008	0.0128 ± 0.000069	-0.00021 ± 0.000236	0.001532 ± 0.000017	2.63E-14	89.7%	4.0447	28.16 ± 0.05	1.83E-03
102	2.6	15	3.61312 ± 0.002736	0.85825 ± 0.001140	0.0111 ± 0.000046	-0.00048 ± 0.000341	0.000394 ± 0.000013	2.15E-14	96.8%	4.0742	28.37 ± 0.05	1.92E-03
103	2.6	15	5.37008 ± 0.001955	1.23703 ± 0.001437	0.0167 ± 0.000163	0.00031 ± 0.000331	0.001413 ± 0.000024	3.20E-14	92.2%	4.0036	27.88 ± 0.05	1.97E-03
104	2.6	15	9.56457 ± 0.007605	2.14855 ± 0.001151	0.0291 ± 0.000116	0.00027 ± 0.000308	0.003121 ± 0.000047	5.69E-14	90.4%	4.0224	28.01 ± 0.05	1.91E-03
105	2.6	15	6.87806 ± 0.008032	1.31300 ± 0.001860	0.0183 ± 0.000111	-0.00007 ± 0.000411	0.004529 ± 0.000062	4.09E-14	80.5%	4.2192	29.37 ± 0.12	4.01E-03
106	2.6	15	7.47048 ± 0.002579	1.55511 ± 0.001932	0.0210 ± 0.000176	0.00026 ± 0.000248	0.002924 ± 0.000024	4.45E-14	88.4%	4.2483	29.57 ± 0.05	1.82E-03
107	2.6	15	12.10149 ± 0.005636	2.48813 ± 0.002155	0.0332 ± 0.000110	0.00304 ± 0.000216	0.005414 ± 0.000032	7.20E-14	86.8%	4.2208	29.38 ± 0.04	1.46E-03
108	2.6	15	6.36445 ± 0.005320	1.33645 ± 0.001553	0.0176 ± 0.000104	0.00045 ± 0.000318	0.002758 ± 0.000023	3.79E-14	87.2%	4.1525	28.91 ± 0.06	2.05E-03
109	2.6	15	9.81300 ± 0.008147	2.02096 ± 0.002533	0.0272 ± 0.000179	0.00088 ± 0.000378	0.004353 ± 0.000027	5.84E-14	86.9%	4.2191	29.37 ± 0.06	1.97E-03
110	2.6	15	7.27592 ± 0.006797	1.57145 ± 0.001666	0.0210 ± 0.000183	0.00015 ± 0.000267	0.002766 ± 0.000021	4.33E-14	88.8%	4.1100	28.62 ± 0.05	1.85E-03
113	2.6	15	6.09567 ± 0.003174	0.94144 ± 0.000598	0.0134 ± 0.000092	0.00060 ± 0.000350	0.006362 ± 0.000061	3.63E-14	69.2%	4.4779	31.15 ± 0.14	4.43E-03
114	2.6	15	7.29015 ± 0.006832	1.45704 ± 0.001595	0.0192 ± 0.000117	-0.00046 ± 0.000411	0.002456 ± 0.000024	4.34E-14	90.0%	4.5052	31.34 ± 0.06	1.94E-03
115	2.6	15	2.40743 ± 0.001333	0.56105 ± 0.000951	0.0074 ± 0.000077	0.00032 ± 0.000200	0.000241 ± 0.000015	1.43E-14	97.0%	4.1638	28.99 ± 0.08	2.68E-03
116	2.6	15	6.84487 ± 0.004524	1.44102 ± 0.001269	0.0197 ± 0.000117	0.00021 ± 0.000427	0.003345 ± 0.000023	4.07E-14	85.6%	4.0642	28.30 ± 0.05	1.75E-03
117	2.6	15	7.15321 ± 0.005234	1.33390 ± 0.002105	0.0188 ± 0.000136	0.00077 ± 0.000207	0.005881 ± 0.000061	4.26E-14	75.7%	4.0598	28.27 ± 0.12	4.09E-03
118	2.6	15	9.19695 ± 0.006400	1.81613 ± 0.002530	0.0247 ± 0.000186	0.00074 ± 0.000327	0.005430 ± 0.000031	5.47E-14	82.6%	4.1805	29.10 ± 0.07	2.26E-03